



Dipartimento di Medicina Clinica e Chirurgia
Università di Napoli Federico II

Dottorato in Terapie avanzate medico-chirurgiche

Emery Di Cicco
(XXXII° CICLO)

**Thyroid hormone signaling in epithelial tumors: Role of type
2 deiodinase in the progression of Squamous cell Carcinoma**

Tutor: Prof. Monica Dentice

INDEX

SUMMARY	3
1.INTRODUCTION	4
1.1 THE ORIGINS OF SQUAMOUS CELL CARCINOMA	4
1.2 CUTANEOUS SCC	5
1.3 TUMOR INITIATING CELLS (TICs): A MODEL OF SECONDARY TUMOR FORMATION	6
1.4 THE MECHANISM OF EPITHELIAL MESENCHYMAL TRANSITION DURING TUMOR PROGRESSION AND METASTASIS	7
1.5 THYROID HORMONES ACTION AND DEIODINASES.	8
1.6 DEIODINASES D2 AND D3 IN CANCER.	10
2. AIM OF THE PROJECT.	12
3. RESULTS	13
4.DISCUSSION	22
5.METHODS	24
6. SUPPLEMENTARY INFORMATIONS	31
7.REFERENCES	41

Summary

Epithelial tumorigenesis is a multistep process that promotes the progression from normal epithelial cells to clinically evident cancerous lesions capable of producing metastases. Cutaneous Squamous Cell Carcinoma (cSCC) is one of the most common cancer in humans that rarely metastasize, but metastasis is associated with a poor prognosis, with a low patient survival rate. Thyroid hormone (TH) plays a key role in the regulation of many biological processes including cell proliferation, differentiation and survival. In the target tissues, the concentration of TH is regulated by the actions of the deiodinases D2 and D3, which are viewed as a cell-specific pre-receptor mechanism to control thyroid hormone signaling that cannot be predicted based on the levels of circulating thyroid hormone. The association between dysregulation of TH signaling and human cancer was largely demonstrated. In the last years, our group provided the evidence of a functional link between the TH modulating enzymes, deiodinases, and non-melanoma skin cancer (NMSC) formation. In particular, we demonstrated that: i) D3 is overexpressed in basal cell carcinomas (BCCs) and is under the control of Hedgehog pathway; ii) TH treatment reduces tumor growth by attenuating the oncogenic potential of BCC tumor drivers Shh and miR21; iii) BCC cells express also D2 and the anti-tumorigenic action of TH in BCC can be attributed to its ability to reduce tumor cell proliferation, and increase the apoptotic rate. Although these evidences, the effective role of TH D2-produced in the progression of epithelial tumorigenesis was never been clarified. In this project, we described that intracellular activation of TH signaling by D2 enhances malignant evolution of SCCs, promoting epithelial-mesenchymal (EMT) transition of cancer cells. Accordingly, second tumors that expresses high level of D2, show aggressive phenotype and infiltration at distant sites. In human SCC, elevated D2 correlates with tumor grade and is associated with an increased risk of postsurgical relapse and shorter disease-free survival. These data provide the first in vivo demonstration of the effective role of TH and its activating enzyme, D2, not only in the EMT, but also in the metastatic transformation and open new opportunities in the therapeutic field.

1.Introduction

1.1 The origins of Squamous Cell Carcinoma

Squamous cell carcinomas (SCCs) are among the most frequent solid cancers in humans [1] and represent a major cause of death worldwide. Their incidence is sharply rising owing to increased exposure to carcinogens, such as ultraviolet radiation related to sun exposure, smoking, alcohol consumption or human papilloma virus (HPV) infection [1] [2]. SCCs are classified according to the location where they appear, being frequently found in skin, head and neck, esophagus, lung and [2] [3] [4] [5] and more rarely in pancreas, thyroid, bladder and prostate [6] [7]. Development of these tumors is linked closely to genomic perturbations, genetic mutations, and/or altered expression of key molecules involved in various stages of squamous cell lineage commitment and/or terminal differentiation. Alterations of underlying stromal cells also play an important role in the development of these tumors, and recent evidence indicates that they may even be a primary determinant, besides promoting escape from immune surveillance and resistance to chemotherapy [8] [9]. A distinguishing feature of SCCs is their high degree of cellular heterogeneity, with cell populations at various stages of differentiation, which are able to reverse lineage commitment to proliferative stages as well as enter into quiescent, slow-cycling growth phases. These features make them particularly difficult to target with monotherapeutic approaches [10].

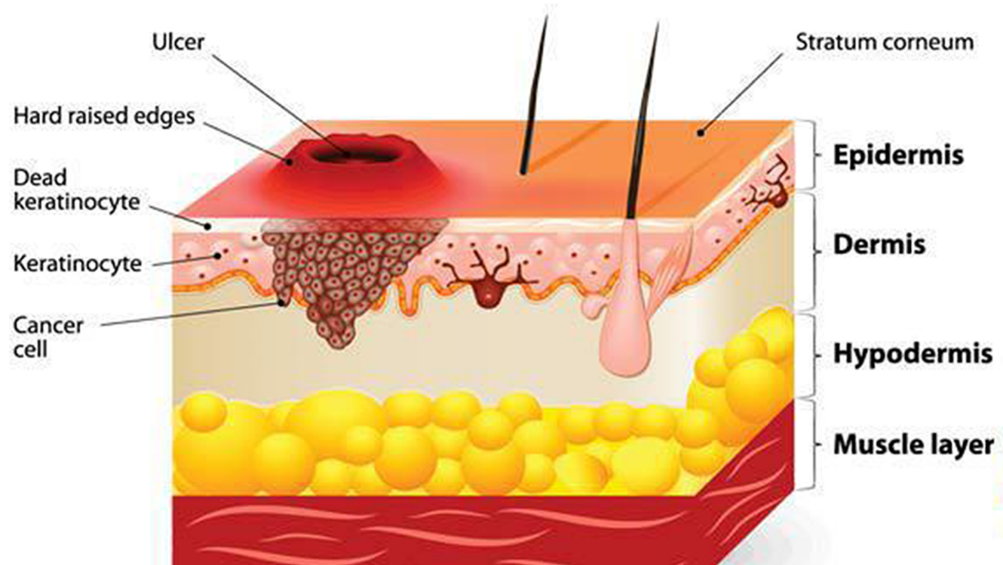


Figure A. Schematic representation of SCC

1.2 Cutaneous SCC (cSCC)

cSCC is one of the most common cancers in humans, accounting for over 700,000 new patients per year in the United States [11]. cSCCs rarely metastasize (5%), but metastasis is associated with a poor prognosis, with a patient survival of 10–20% over 10 years [2]. Sun exposure, chronic wounds and immune suppression are the major risk factors of cSCC. Actinic keratosis (human) and papilloma (mouse) represent benign squamous lesions that progress into malignant cSCCs. Mouse models for skin squamous tumors resemble human skin cancers and offer an ideal model to study cancer initiation and growth [12] [13]. The most extensively used mouse model for cSCC is a carcinogen-induced protocol consisting of a topical application of DMBA, a mutagen, followed by administration of TPA, which stimulates epidermal proliferation and inflammation [14]. In the first step (called ‘initiation’), mice are treated with a low dose of the mutagen 9,10-dimethyl-1,2-benzanthracene (DMBA). In the second step (called ‘promotion’), mice are treated with 12-Otetradecanoyl phorbol-13-acetate (TPA), a drug that stimulates epidermal proliferation. During promotion, benign tumors (papilloma) arise, some of which progress to invasive SCC. DMBA–TPA-induced cSCC is almost invariably (>90%) associated with mutations in RAS family members, most frequently Hras,

followed by Kras and Rras [15] [16] [17]. Human SCCs present a high degree of cellular heterogeneity, varying from well-differentiated to poorly differentiated tumors, which present a higher rate of recurrence and lower rate of cure after treatment [2].

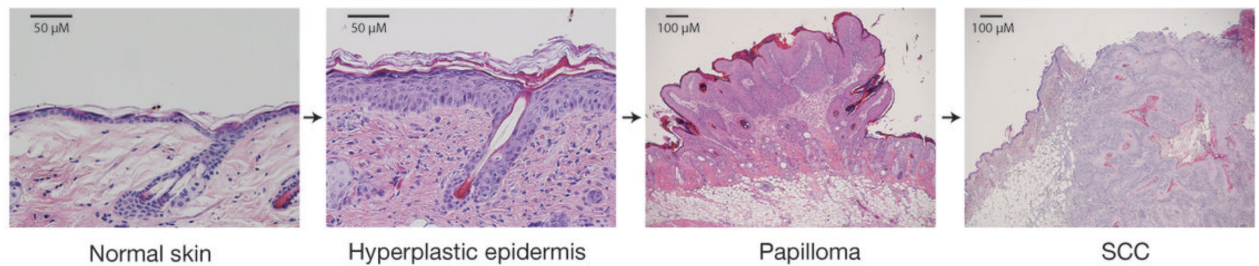


Figure B. Two-stage model of skin carcinogenesis in mice, *Abel et al, 2009 Nat. Protoc.*

1.3 Tumor initiating cells (TICs): a model of secondary tumor formation

Different models have been proposed to explain tumor growth and heterogeneity. In the stochastic model of tumor growth, all cancer cells have the same intrinsic properties to contribute to tumors growth and choose between self-renewal and differentiation in a stochastic manner [18] [19]. In contrast, in the cancer stem cell (CSC) model, tumors are hierarchally organized, with only some tumor cells, called CSCs, presenting greater renewing potential that sustain long-term tumor growth [20] [18] [19]. Many recent studies using prospective isolation of a fraction of tumor cells followed by their transplantation into immunodeficient mice have demonstrated that certain population of tumor cells contains cells with higher probability to reform secondary tumor upon transplantation, supporting the existence of CSC [20] [21] [22]. Furthermore, the existence of CSCs in different types of primary solid tumors, including skin squamous tumors, has recently been confirmed by lineage-tracing experiments [23, 24]. Recently, CD34-expressing tumor propagating cells (TPCs) with increased clonogenic potential and the ability to form secondary tumors upon transplantation into immunodeficient mice have been isolated from DMBA/TPA-induced skin SCC [25].

1.4 The mechanism of epithelial mesenchymal transition during tumor progression and metastasis

Epithelial–mesenchymal transition (EMT) is a cellular process in which cells lose their epithelial characteristics and acquire mesenchymal features. EMT has been associated with various tumor functions, including tumor initiation, malignant progression, tumor stemness, tumor cell migration, intravasation to the blood, metastasis, and resistance to therapy [26, 27]. EMT has long been viewed as a binary process with two distinct cell populations, epithelial and mesenchymal [26] [28], and is often defined by the loss of the epithelial marker E-cadherin and the gain of the expression of the mesenchymal marker vimentin. However, recent studies indicate that EMT occurs in a gradual manner characterized by several cellular states expressing different levels of epithelial and mesenchymal markers and exhibiting intermediate morphological, transcriptional, and epigenetic features, between epithelial and mesenchymal cells [29] [30]. The intermediate states between epithelial and fully mesenchymal states have been referred to as partial, incomplete, or hybrid EMT states. Transcriptional profiling of the different tumor cell populations arising in SCCs presenting EMT revealed that some markers traditionally used to define epithelial state such as *Cdh1* or *EPCAM* were lost in the early step of EMT, while others such as *Krt14*, *Krt5*, or *Krt8* were completely lost in the late stages of EMT [31]. Similarly, mesenchymal markers exhibited different patterns of expression: some known EMT genes and TFs, such as *Cdh2*, *Vim*, *Snai1*, *Twist1/2*, and *Zeb1/2* were highly upregulated in early hybrid states and were maintained at the same level in the more mesenchymal populations, while the expression of *Cdh11*, *Pdgfra*, *Pdgfrb*, *Fap*, *Loxl1*, *Col24a1*, *Mmp19*, or *Prrx1* increased in late stages of EMT. EMT has been also associated with tumor stemness by their increased tumor propagating potential following their transplantation into immunodeficient mice. Forced expression of TFs that promote EMT such as *Twist1* or *Snail1* in mammary epithelial cells increase their ability to give rise to secondary tumors upon transplantation [32] [33].

Tumor metastasis is the most common cause of death in cancer patients. In carcinomas, the metastatic process is thought to consist of a number of distinct steps. The first step *invasion* requires neoplastic epithelial cells to lose cell-cell adhesion and to gain motility, which enables them to invade the adjacent tissue. During the second step, intravasation, tumor cells penetrate through the endothelium of blood or lymphatic vessels to enter the systemic circulation. Only some circulating tumor cells appear to be able to survive the

passage through circulation. Some of these survivors manage to complete the next step *extravasation* as they extravasate through the capillary endothelium at distal sites. Finally, in the new host environment, an even smaller subset of such metastasizing cells succeeds in proliferating from minute growths (micrometastases) into malignant, secondary tumors [34].

1.5 Thyroid hormones action and deiodinases.

T4 and its most biologically active metabolite T3 are diffuse endocrine molecules that influence such aspects of cellular physiology as cellular growth, differentiation and apoptosis. Their plasmatic concentration is strictly regulated by the hypothalamic-pituitary-thyroid (HPT) axis. In response to different stimuli, the hypothalamus generates TRH, which induces the secretion of TSH from the pituitary, this in turn stimulates the thyroid gland to release T4 and T3 thyroid hormones, (THs) into the circulation. On the other hand, serum TH provides an additional regulatory control by exerting negative feedback effects on the axis at both pituitary and hypothalamic level. Despite the relatively constant TH plasma levels, tissues can undergo remarkable changes in TH concentration consequent to local TH metabolism, which ultimately controls the TH signature at gene expression level. This is achieved through several mechanisms, namely transport across the cellular membrane, iodothyronine deiodinase activity, expression of various nuclear receptor isoforms and their interaction with DNA and chromatin modifier proteins. Once inside the cell thanks to monocarboxylate transporters (MCTs), anion-transporting polypeptides (OATPs) and the L-type amino acid transporters LAT1 and LAT2 [35]., most of the actions of T3 are mediated by the thyroid hormone receptors (TRs).

Within the cytosol, the deiodinases exert a major metabolic control of TH concentration. Iodothyronine deiodinase types I, II and III (D1, D2 and D3, respectively) constitute a family of selenoenzymes that activate and inactivate THs through the removal of specific iodine moieties from thyroxine and its derivatives. Whereas D1 and D2 activate T4 by converting it into T3, D3 converts both T4 and T3 into inactive metabolites by removing an iodine atom from the inner ring of these molecules [36]. These enzymes are expressed in many tissues and constitute the major mechanisms of cell-autonomous, pre-receptor

control of TH action. The expression of activating and inactivating deiodinases plays a pivotal role in a number of mammalian tissues, including the central nervous system, from development to the adult state [36]. The action of D2 and D3 is finely regulated in the way to coordinate TH action in various tissues. D2 is considered the main T4-activating enzyme, given its high substrate affinity. D2 is a classical type-1 membrane protein, approximately of 31 kDa, residing on the endoplasmic reticulum (ER) membrane, with a half-life of ~ 45 minutes [37]. Its relatively short half-life is due to ubiquitination and proteasome uptake, a feature that is accelerated by D2 interaction with its natural substrate, T4 [38]. D2 is expressed in many brain areas and is considered to play a major role in local T3 production in the brain. D2 is also expressed in pituitary, brown adipose tissue, placenta, skeletal muscle and skin [36] [39]. The preferred substrate for D2 is T4 and, although to a lesser extent, rT3. D2 is regulated by thyroid hormones both pre- and post-transcriptionally as T3 downregulates D2 mRNA expression [40], while T4 as well as rT3 (the substrates of D2) increase D2 ubiquitination and subsequently proteasomal degradation, resulting in decreased D2 activity. The Dio3 gene encodes the D3 protein, a 32-kDa selenoprotein that contains a Sec residue within the catalytic center [41]. In vertebrates, D3 is highly expressed during development and, although its expression decreases in most tissues in adult life, it persists in few organs, that is, brain, skin, placenta, pregnant uterus and pancreatic b-cells [42] [43] [44]. Being the principal physiological inactivator of TH, D3's main function is to protect tissues from an excess of active hormone. Thyroid hormone excess is among the more potent inducers of D3. It represents a homeostatic negative feedback loop by which TH accelerates its D3-mediated degradation.

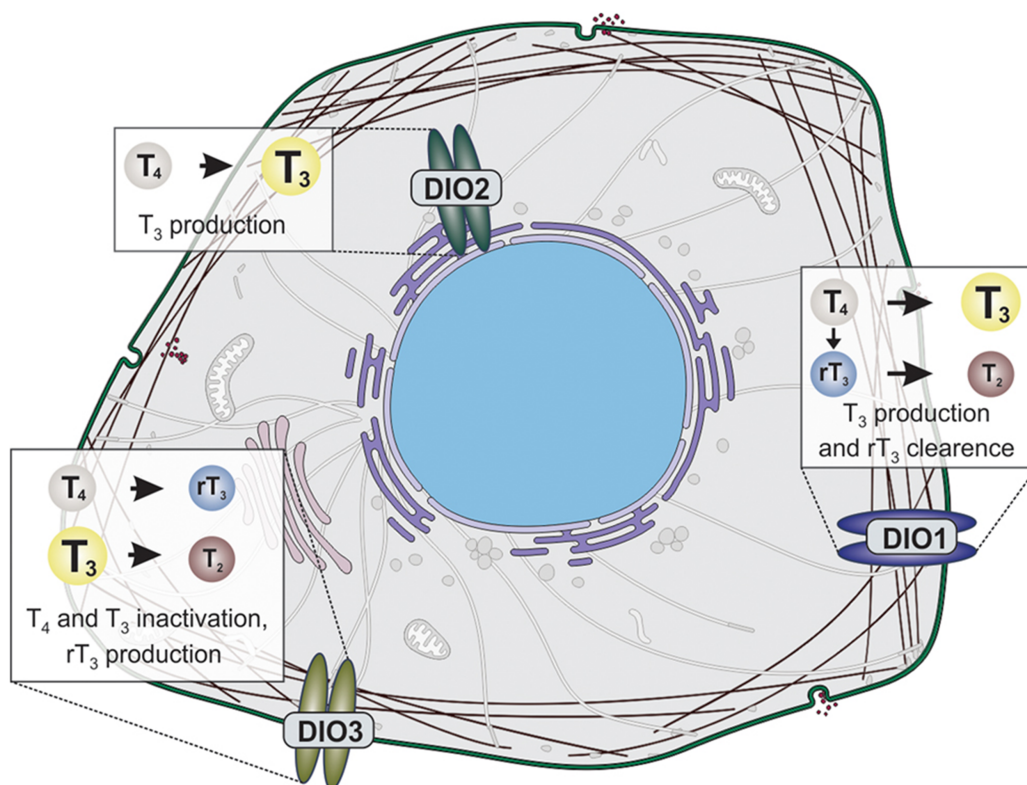


Figure c. Schematic representation of the localization of deiodinases within the cell as well as the main steps of deiodination by which iodothyronines are generated.

Iuri Martin Goemann et al, *Endocrine-Related Cancer* (2019).

1.6 Deiodinases D2 and D3 in cancer.

The association between thyroid hormones and malignancies was first suggested more than a century ago [45]. Thereafter, different clinical studies demonstrated that dysthyroidism can be associated with tumor growth. Moreover, changes in thyroid receptor or deiodinases expression have been reported in several neoplasias [46] [47, 48] [49]. A paradigm of how changes in deiodinases might alter cancer formation is the clinical condition of consumptive hypothyroidism, a severe form of hypothyroidism due to high levels of D3 activity in the neoplastic tissues. It was first described in infantile liver hemangiomas [50]. Subsequently, pediatric and adult liver vascular tumors were also associated with increased expression and activity of D3 [51] [52]. Indeed, large

vascular tumors can express enough D3 sufficient to inactivate a significant amount of plasma T3 and cause overt hypothyroidism. D3 upregulation is induced by the Shh pathway and the MAPK signaling cascade in these types of tumors [53]. *DIO2* and *DIO3* mRNA transcripts, as well as D2 and D3 activities, are present in normal human skin [54] [55]. Several studies on the roles of D2 and D3 in skin cancer demonstrated that Basal cell carcinoma (BCC), which is the most common cutaneous malignancy, expresses high levels of D3 [56, 57] [58] [39, 59]. Our group demonstrated that sonic hedgehog (Shh), through Gli2, directly induces D3 in human and mouse BCCs, reducing intracellular T3 and thus increasing cyclin D1 and proliferation. Shh also mediates D2 reduction through post-transcriptional mechanisms. Thus, D3 knockdown blocks proliferation and reduces the oncogenic potential of BCC tumor cells. It was also demonstrated that T3 has a suppressive effect on the oncogenic microRNA (miRNA) miR21, which in turn induces D3 expression through downregulation of the Grainyhead-like protein 3 homolog (GRHL3) [59]. Therefore, the existence of a miR21/GRHL3/DIO3 axis critically contributes to the intracellular TH imbalance in the context of BCC [59]; thus, BCC is an excellent model to study the TH role in the delicate balance between cell proliferation and differentiation. *DIO2* mRNA has also been demonstrated expressed in these cells. *DIO2*KO-BCC (low intracellular T3) cells are characterized by a high proliferation rate, a high proportion of S-phase cells and decreased apoptosis. This interesting model could be expanded to other neoplasias aiming for a better understanding of the effects of THs on cancer [39].

The role of D2 in cancer was also investigated during the years, and these studies revealed D2 expression is much higher in most brain tumors such as astrocytoma and glioblastoma with the highest D2 activity in gliosarcomas and oligodendrogliomas [60] [61] [62].

D2 mRNA levels in 105 pituitary tumors were also found to be increased in all pituitary tumors with the highest expression observed in non- functional adenoma when compared with normal pituitary tissue. Furthermore, several neoplastic cell lines were found to exhibit high D2 expression as compared with their normal counterparts. For example, D2 is usually expressed in placenta and is also present in JEG3, a choriocarcinoma cell line [63]. In these cells, D2 has been shown to be highly responsive to cAMP treatment that involves the binding of transcription factor CRE binding protein (CREB) to the CRE located in the hD2 promoter [63]. At the same time, D2, which is expressed in mesothelial

cells, has higher expression in the mesothelioma cell line (MSTO-211H), with the highest levels of D2 ever seen in cultured cells [64]. The expression of D2 mRNA and the presence of D2 activity were detected also in human osteoblast-like osteosarcoma (SaOS-2) cell line but this time in lower amount compared with the normal human osteoblast (NHOst) cells [65].

2. Aim of the project.

Squamous cell carcinomas (cSCC) represent the most aggressive type of nonmelanoma skin cancer. SCC carcinogenesis is a complex multistep process that involve the progression from normal epithelial cells to malignant cancerous lesions capable of producing metastases [66]. Over the years, it was largely described that alterations in TH signaling influences the oncogenic processes of epithelial tumors [58] [67] [57] [59] [39]. At tissue level, TH action is regulated by the expression and activity of three seleno-deiodinases, which catalyze TH activation (D1 and D2) and catabolism deiodinases (D3). Most of the studies on deiodinases in cancer highlighted the role of D3 in the regulation of cancer cell proliferation in epithelial tumors, focusing on the first stages of tumor formation. Conversely, it was not clarified the role of TH signaling in the tumor progression and metastatic conversion. Based on these considerations, **my PhD aimed to determine the effects of TH signaling and its regulators in the late stages of the neoplastic process, and specifically to investigate how D2 regulates SCC progression, invasion and metastatic conversion in both mouse and human cancers.**

3. Results

D2 expression correlates with aggressive secondary tumors.

To investigate the role of TH signaling during tumor progression, we analyzed the expression of deiodinases D2 and D3 using an alternative model of SCC tumorigenesis, namely transplantation of tumor initiating cells (TICs) into immunodeficient-athymic mice. We isolated TICs by FACS sorting of $\text{Lin}^-/\alpha\text{-6integrin}^+/\text{Epcam}^+/\text{CD34}^+$ cells from SCC tumors, that we previously obtained using chemical two-step carcinogenesis [14] (Figure 1A). These cells form secondary tumors upon transplantation [68]. Ten weeks after transplantation, mice developed palpable tumors (Type I tumors), which progressed and assumed a SCC-like phenotype 16 weeks after transplantation (Type II tumors) (Figure 1B). Lymph node morphology differed between type I and type II tumor-bearing mice (Figure 1B). Interestingly, while the expression of D2 and D3 increased to a similar extent in the transplanted TIC cells, their expression conversely fluctuated as the tumors developed. In detail, D3 expression was enhanced in type I tumors, whereas D2 was enhanced and predominated in type II tumors and in lymph nodes from mice bearing type II tumors (Figure 1C and Supplemental Figure 1). These data are in line with the concept that D3 is upregulated during tumor growth thereby attenuating TH signal in benign tumors (papillomas), while D2 expression is upregulated in more aggressive and infiltrating cancer cells thereby enabling TH signal amplification at the EMT and progression to a higher tumor grade.

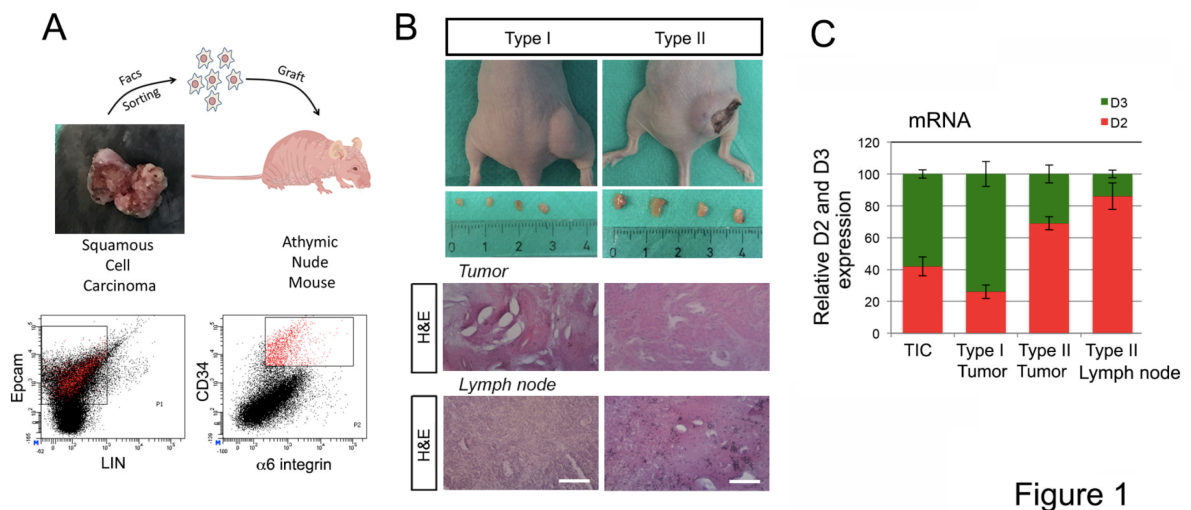


Figure 1

Figure 1. Tumor xenografts from tumor-initiating cells transplantation dynamically express D2 and D3 during tumor progression. a Schematic representation of the strategy used to isolate and graft TICs from DMBA/TPA tumors (n = 6). b Representative images of tumors and lymph nodes generated in athymic mice 10 (type I) and 16 (type II) weeks after transplantation (Top). H&E of the tumors and lymph nodes in type I and II mice. Scale bars represent 100 μ m (Bottom). c Relative expression of D2 and D3 in type I and II tumors and in lymph nodes measured by real-time PCR.

Attenuation of TH signaling reduces tumor invasion

To gain insight into the role of TH in tumor progression, we disrupted the TH signal balance by depleting D2 in the epidermal compartment. To this end, we crossed the D2^{fl/fl} [69] mice with K14Cre^{ERT} mice [68]. [68]. SCC tumors were induced by treating the sD2KO mice with the classical chemical carcinogenesis model, namely “two-stage” chemical carcinogenesis [14]. In the first, initiation step, mice were treated with the mutagen DMBA; in the second promoting step, mice were treated with 12-O tetradecanoyl- phorbol-13-acetate (TPA), a drug that stimulates epidermal proliferation and inflammation. To evaluate tumor progression in an epidermal-specific D2KO background (sD2KO), we depleted D2 from the epidermal compartment by administrating tamoxifen before the DMBA/TPA treatment and analyzed the skin lesions 20 weeks later (Figure 2A). As shown in Figure 2B, C, D2-depletion increased the

frequency of hyperplastic lesions and papillomas. sD2KO mice developed skin papillomas at an average of 10 weeks after the first application of DMBA, compared with 14 weeks in control mice (Figure 2B). By week 20, 100% of sD2KO mice and only 70% of control mice developed tumors. D2-depletion increased the level of K6 in D2KO papillomas, which confirms that lowering the level of T3 by D2-depletion accelerates tumor growth (Figure 2D, E). Notably, the greater tumor growth in D2KO mice was not associated with greater tumor progression and invasive conversion. Indeed, as shown in Figure 3D and E, K8 expression was lower in sD2KO mice than in control mice, which indicates that D2KO papillomas resist progression to SCC. The lower propensity of sD2KO tumors to acquire a more invasive phenotype was confirmed by the higher E-cadherin/N-cadherin ratio in sD2KO tumors (Figure 2D, E). This finding demonstrates that TH attenuation via D2-depletion reduces the EMT, and that, while increasing tumor formation, it slows tumor progression. To assess the impact of D2-depletion at later stages of tumor progression, we removed D2 from the epidermal compartment 20 weeks after DMBA treatment and analyzed tumor behavior thereafter (Figure 2F). In this case, the total number of tumors was similar in the sD2KO and control mice. However, while tumors in control mice evolved towards a carcinoma-like phenotype (Figure 2F), tumor progression was delayed in the sD2KO mice. Indeed, by week 25, sD2KO mice developed an average of 1.1 carcinoma-like, large tumors (>3 mm) per mouse compared with 4.4 large tumors per mouse in their control littermates ($P < 0.01$; Figure 2G, H). Moreover, K8 levels were lower in sD2KO mice than in control mice (Figure 2I), which suggests that D2 expression and TH activation is an essential component of the shift from a papilloma grade to a more invasive SCC (Figure 2L).

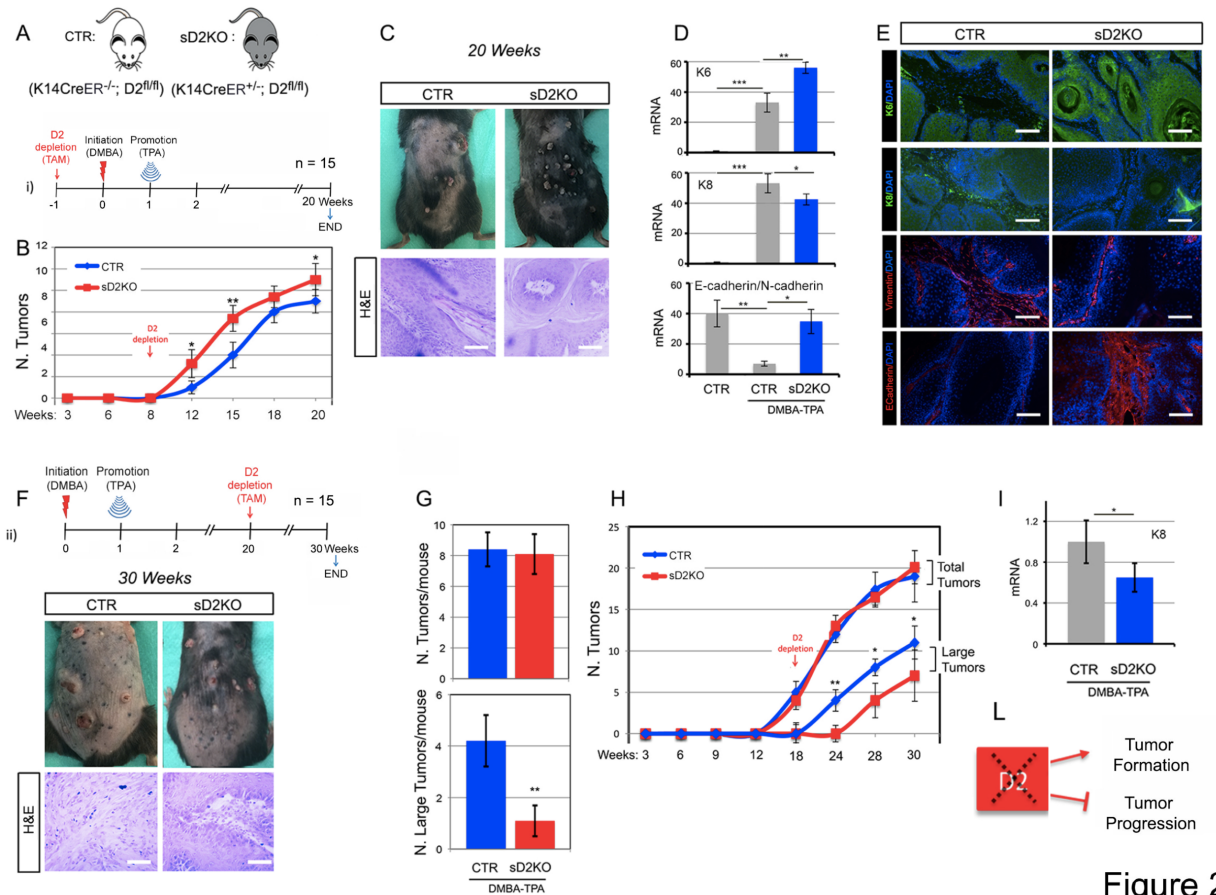


Figure 2

Figure 2. Attenuation of TH signaling in D2KO mice enhanced tumor growth and reduced the EMT. a Schematic representation of D2-depletion and the two-step carcinogenesis experiment in 15 CTR and 15 sD2KO samples (n = 15). b The number of skin lesions counted during DMBA/TPA treatment in sD2KO and CTR mice. c Picture of the dorsal skin from CTR (n = 15) and sD2KO (n = 15) mice treated with DMBA/TPA for 20 weeks showing papillomas and advanced SCC (top). H&E of the skin lesions from CTR (n = 8) and sD2KO (n = 12) mice (bottom). Scale bars represent 200 μ m. d The mRNA levels of K6, K8, and E-cadherin/N-cadherin ratio in skin lesions of CTR (n = 15) and sD2KO (n = 15) mice measured by real-time PCR analysis. e Immunostaining for K6, K8, vimentin, and E-cadherin was performed on paraffin-embedded sections of dorsal skin lesions (n = 10 for both groups). Scale bars represent 200 μ m. f Schematic representation of D2-depletion from the epidermal compartment at the end of DMBA/TPA treatment (top, n = 15). Representative pictures and H&E staining of skin lesions from sD2KO (n = 12) and CTR (n = 8) mice treated with DMBA/TPA for 30 weeks (bottom). Scale bars represent 200 μ m. g and h The number of tumors (detectable tumors, >1 mm) and number of large tumors (> 3 mm) counted during DMBA/TPA

treatment in sD2KO and CTR mice. i mRNA levels of K8 in skin lesions of CTR (n = 15) and sD2KO (n = 15) mice measured by real-time PCR analysis. *P < 0.05, **P < 0.01, ***P < 0.001. j Schematic representation of the effects of D2-depletion on SCC tumor growth and progression.

Intracellular T3 induces epithelial-mesenchymal transition

Given the effects of D2-depletion in SCC progression and invasiveness, we investigated whether the TH signal is a positive regulator of the invasive conversion of cancer cells. Consequently, we evaluated the contribution of the TH signal to the promotion of the EMT in the human skin squamous cell carcinoma SCC 13 cells. As shown in Figure 3A, T3 treatment increased N-cadherin expression and slightly reduced E-cadherin expression, thereby resulting in a net attenuation of the E-cadherin/N-cadherin ratio, which indicates an increased EMT profile. We also measured the expression of two other EMT markers namely, vimentin and Twist, and found that both were positively regulated by T3 (Supplementary Figure 2A). To explore the role of the intracellular control of TH action in EMT, we suppressed D2 or D3 expression in SCC 13 cells using CRISPR/Cas9 technology. D2-depletion and D3-depletion were verified by gene sequencing and PCR analysis, respectively (Supplementary Figure 3). Western blot revealed that D3-depletion (which increases intracellular T3) phenocopied the effects exerted by T3 on the EMT. Indeed, the E-cadherin/N-cadherin ratio at mRNA and protein level was reduced in D3KO cells and in T3-treated cells (Figure 3B and Supplementary Figure 2C). Accordingly, the E-cadherin/N-cadherin ratio was elevated in D2KO cells versus control cells (Figure 3C and Supplementary Figure 2C). The expression of the EMT markers vimentin and Twist was also inversely regulated in D2KO cells versus D3KO cells (Supplementary Figure 2B). Vice versa, vimentin and Twist were induced in D2 overexpressing SCC cells and downregulated in D3 overexpressing SCC cells (Supplementary Figure 4). D3-depletion and T3 treatment of SCC cells caused a morphological shift, namely, delocalization of phalloidin from the membrane to the cytoskeleton, an increase of vimentin expression and a decrease of E-cadherin expression (Figure 3D, E). Notably, T3 reduced SCC cells proliferation (Figure 3F), which confirms its effects as an anti-proliferative agent in SCC, but contextually, it enhanced the migration of SCC cells (Figure 3G). Accordingly, D3-depletion in D3KO cells caused

growth attenuation, but enhanced migration (Supplementary Figure 5A, C), whereas D2KO cells had the opposite profile, i.e., increased proliferation (Supplementary Figure 5B) and reduced migration (Supplementary Figure 5C). To assess whether T3 induced invasiveness as well as migration, we performed a transwell invasion assay and found that T3 significantly increased the invasiveness of SCC cells (Figure 3H). Since T3 induced matrix degradation (Figure 3H), we extended the analysis to metalloproteases, which are important inducers of invasiveness and of the EMT. We analyzed the expression patterns of a panel of seven metalloproteases (MMP 2, 3, 7, 8, 9, 10 and 13) in D3KO and D2KO cells versus control cells. Real time PCR analysis revealed that the expression of MMP 2, 3, 7 and 13 was higher in D3KO cells, and lower in D2KO cells than in controls (Supplementary Figure 6A). Accordingly, secretion in the culture medium and the enzymatic activity of metalloproteases 2, 3, 7 and 13 were robustly increased in D3KO and reduced in D2KO cells (Supplementary Figure 6B and C). These results show that TH acts as an up-stream regulator of cell matrix degradation and of the cell invasion process.

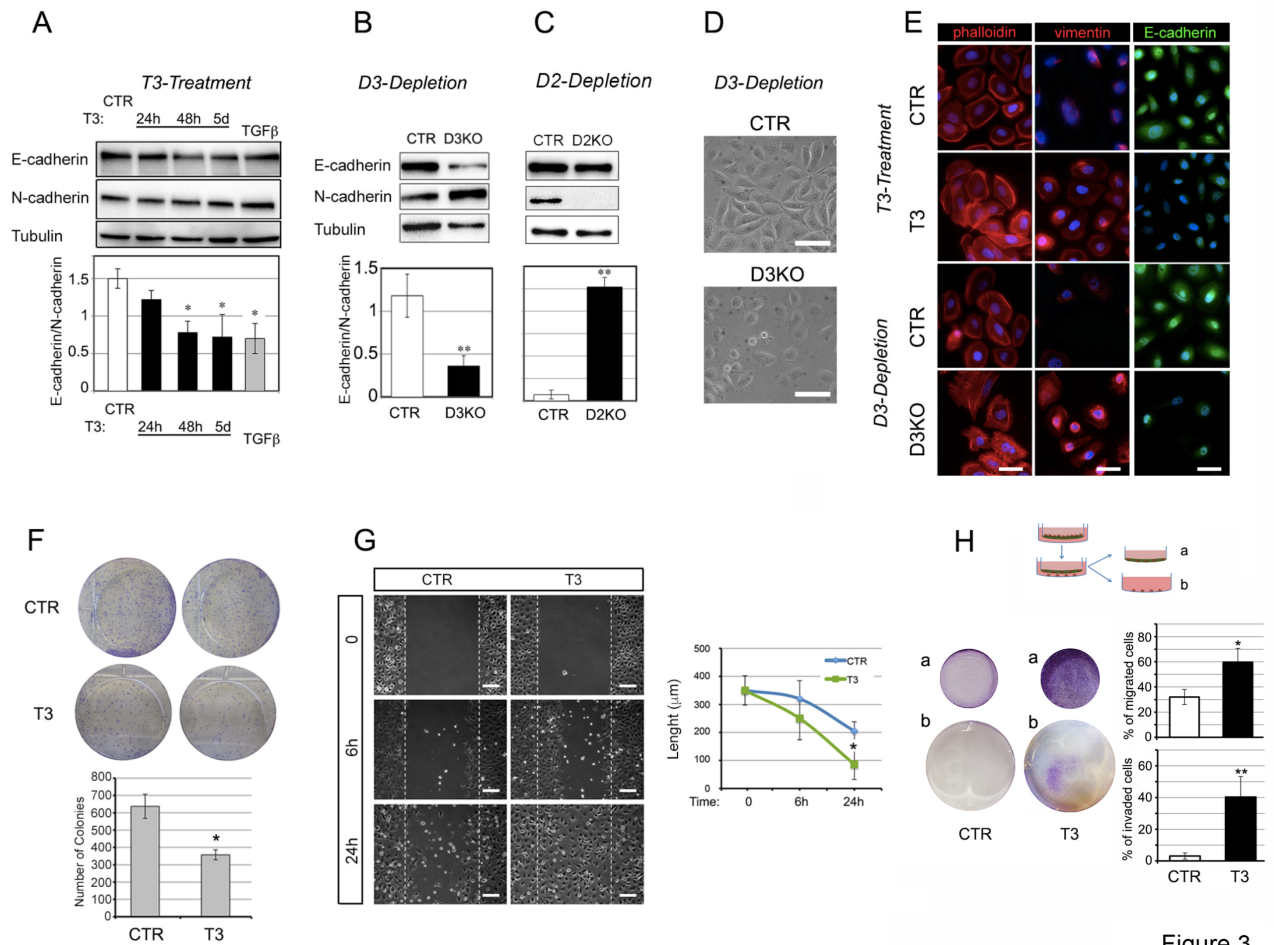


Figure 3

Figure 3. *Thyroid hormone activation induces the epithelial-mesenchymal transition and migration and invasion ability of SCC cells.* (A) SCC cells were treated with 30 nM T3 for different time points or with 5ng/□l TGF□ for 48 h. Total protein lysates were used for western blot analysis of E-cadherin and N-cadherin expression. Tubulin expression was measured as loading control. One representative immunoblot of seven is shown (top). Quantification of the E-cadherin/N-cadherin ratio in the western blot is represented by histograms. (B) Western blot analysis of E-cadherin and N-cadherin expression performed as indicated in (A) in SCC-CTR and SCC-D3KO cells. (C) Western blot analysis of E-cadherin and N-cadherin expression in SCC-CTR and SCC-D2KO cells. (D) Representative phase contrast of CTR and D3KO cells. Scale bars represent 50 □m. (E) Phalloidin (red), Vimentin (red) and E-cadherin staining (green) of untreated and T3-treated SCC cells, SCC-CTR cells and SCC-D3KO cells. One representative experiment of 5 is shown. Scale bars represent 50 □m. * $P < 0.05$, ** $P < 0.01$. (F) Cell proliferation was assessed by colony assay of SCC cells treated or not with 30 nM T3 (top). The

number of colonies formed 8 days after plating shown by scale bars (Bottom). One representative assay of five is shown. **(G)** Wound scratch assay was performed in SCC cells after treatment with T3 (30 nM) for 0, 6 and 24 hours. Cell migration was measured as described in Materials and Methods. Scale bars represent 200 μ m. **(H)** Invasion assay performed on SCC cells treated or not with 30 nM T3 for 5 days. **b** represents cells that invaded on the receiver plate and the area covered by invaded cells is indicated. The percentage of cells that migrated and invaded are represented by histograms.

D2 depletion attenuates metastatic formation

To study the role of T3 in metastatic formation, we first evaluated whether D2 is expressed in metastatic lesions at distant sites. Metastatic lesions in the lung of D2-3xFlag mice treated with DMBA/TPA were positive for D2, as demonstrated by double staining of D2/CXCR-4 and D2/K8 (Figure 4A). D2 and K8 mRNA were potently expressed in lymph nodes and lung metastasis, while D3 was barely detectable in metastatic lesions (Figure 4B). Moreover, the number of metastatic lesions in liver, lung and lymph nodes in D2KO, D3KO and control mice treated with DMBA/TPA for 20 and 30 weeks was higher in D3KO mice and lower in D2KO mice versus control mice (Figure 4C).

D2 is a prognostic marker of human SCC progression

Since our general hypothesis is that transformation of benign papillomas to invasive SCC is causally linked to D2-mediated T3 activation, we evaluated the correlation of D2 expression in human tumors using the markers of EMT E-cadherin and ZEB-1, a prime transcriptional factor in the EMT cascade [70], and an up-stream regulator of many EMT-related genes[71], and the relative switch from papillomas to SCC. We collected 72 samples of human tumors at different pathologic states and of diverse tumor grade up to cSCC, to assess the clinical significance of D2 and the TH signal in human SCCs. The tumor stage of each tumor was evaluated by assessing the expression of E-cadherin and ZEB-1 by immunoistochemical assay (n=20) in formalin-fixed paraffin-embedded biopsies of the five stages of the malignant evolution of keratinocytes towards cSCC: normal epidermis, actinic elastosis, advanced actinic keratosis, well-differentiated cSCC and poorly differentiated SCC (Figure 4D) [72]. We then measured the D2 mRNA

expression by real time PCR from the 20 biopsies and found that D2 mRNA was potently overexpressed in cSCC compared to normal epidermis, and that the highest fold change occurred in poorly differentiated cSCC (Figure 4E). Using the X-Tile program[73], we also analyzed previous data from two collections of tumors in which the gene expression signature of SCC was associated to the risk of relapse, recurrence-free survival and overall survival of patients[74] [75]. Kaplan–Meier plots from both data sets showed a striking significant correlation between high D2 levels and risk of relapse, and an inverse correlation with the percent survival of patients (Figure 4F). Taken together, the above results suggest that D2 levels are correlated with a more advanced tumor stage and with a poorer prognosis of human cancers, which suggests that D2 is critical in triggering invasiveness and metastatic spreading of SCCs (Figure 4G). Should this concept be confirmed in other tumor series, it is feasible that distant-site metastasis status can be predicted from D2 gene expression levels, and that D2 might represent a marker in SCC grading procedures.

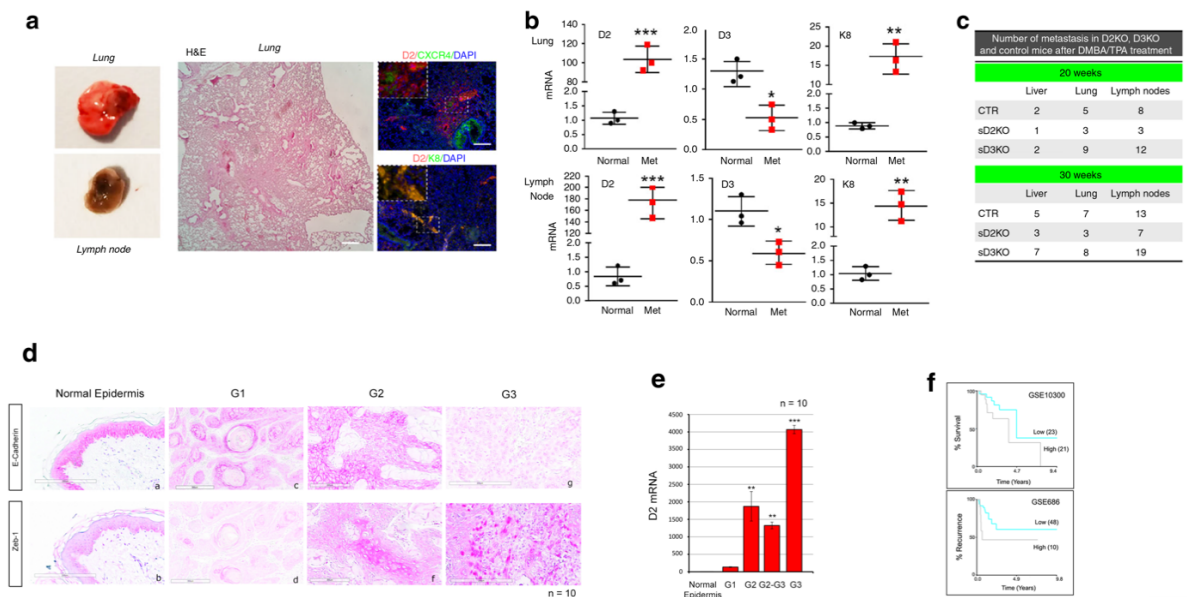


Figure 4

Figure 4. *D2 is expressed in metastatic formations from SCC tumors and its expression in human tumors correlates with a poor diagnosis.* **(A)** Representative images of metastatic lungs and lymph nodes, and H&E, D2/CXCR-4 and D2/K8 co-staining of lung sections from D2-3xFlag mice treated with DMBA/TPA for 24 weeks. Scale bars represent 200 μm . **(B)** Real time PCR analysis of D2, D3 and K8 expression in metastatic lungs and lymph nodes from DMBA-TPA treated mice for 30 weeks (Met) and control, untreated mice (Normal). **(C)** Number of metastatic lesions in sD2KO, sD3KO and control mice 20 and 30 weeks after DMBA/TPA treatment (n=25). **(D)** Representative images showing immunohistochemical (IHC) staining for ZEB-1 and E-cadherin proteins in cutaneous squamous cell carcinoma (cSCC). Positive E-cadherin expression (a) and negative ZEB-1 expression (b) in normal tissue, and in G1 cSCC (d, e). Moderate E-cadherin expression (g) and weak ZEB-1 expression (h) in G2 cSCC. Finally, negative E-cadherin expression (j) and positive ZEB-1 expression (k) in G3 cSCC. IHC analysis was performed in 20 different tissues for each grading. Tumor grading was evaluated as reported in Supplementary Data File 2. **(E)** D2 mRNA levels were measured in human SCC samples at the same grading as in C. * $P < 0.05$, ** $P < 0.01$, *** $P < 0.001$. **(F)** Kaplan–Meier plots from 2 independent data sets (GSE10300 and GSE 686). Blue indicates low and grey indicates high D2 expression. The number of tumors in each group is reported in parentheses.

4. Discussion

Tumor malignancy is linked to tumor heterogeneity and the recurrence often means poor prognosis and increased resistance to therapy [76]. SCC carcinogenesis is a complex multistep process involving the accumulation of several genetic alterations. These alterations promote progression from normal epithelial cells to clinically evident cancerous lesions capable of producing metastases [66]. In this project, we demonstrated that TH activation, via D2 promotes invasiveness and metastatic conversion of SCC in cells in both mouse and human tumors. These data show that D2 expression is upregulated in more aggressive and infiltrating cancer cells thereby enabling TH signal amplification at the EMT and progression to a higher tumor grade. Consequently, our data show that low-TH tumors (D2KO) are fast growing tumors with a low metastatic propensity. Our finding is that the deiodinases system finely regulates TH metabolism in SCC tumors, and specifically D2 promotes the later stages of epithelial tumorigenesis, enhancing cancer cell migration, invasion and metastatic behavior. These evidences are supported by the following results: 1) TH treatment on SCC cells reduces cell proliferation and

enhances cell migration and invasion; 2) SCC cells that express D2 originate more aggressive and infiltrating tumors after transplantation; 3) D2 expression correlates with a more advanced tumor stage and with a poorer prognosis of human cancers. Over the years, it was largely investigated that alterations of TH signaling are associated with human cancer [77]. D2 has frequently been associated with cell differentiation in various cellular contexts [78] [79]. Surprisingly, we recently found abundant D2 expression in BCC and SCC cells – a finding that implicated D2 in epithelial cancer [39]. A search in public databases showed that D2 expression correlates with advanced tumor grading, postsurgical relapse and a shorter disease-free survival. Moreover, the analysis of a panel of 72 human SCC tumors revealed that D2 expression in human tumors is closely associated with more severe and invasive tumors. These data add clinical significance to our study. Indeed, they suggest that D2 expression correlates with such features of malignant tumors as short overall survival, poor prognosis and dismal outcome. These observations reinforce the hypothesis that activation of TH is likely to be a centrally important mechanism for progression of carcinomas to a metastatic stage. In conclusion, in this study we addressed the central question of how TH influences different phases of tumorigenesis. Our data for the first-time link in vitro mechanistic studies with a model of in vivo carcinogenesis in mice, and, importantly also the results of the analysis of human tumors in which all the hypotheses raised based on in vitro studies are confirmed. Therefore, we conclude that D2 is an endogenous “metastasis promoter” and that D2 inhibition can help to reduce human cancer metastasis. These findings not only transform our understanding of how TH influences tumor progression, but also provides the rationale for the concept that pharmacologically-induced TH inactivation could be a strategy with which to attenuate metastatic formations.

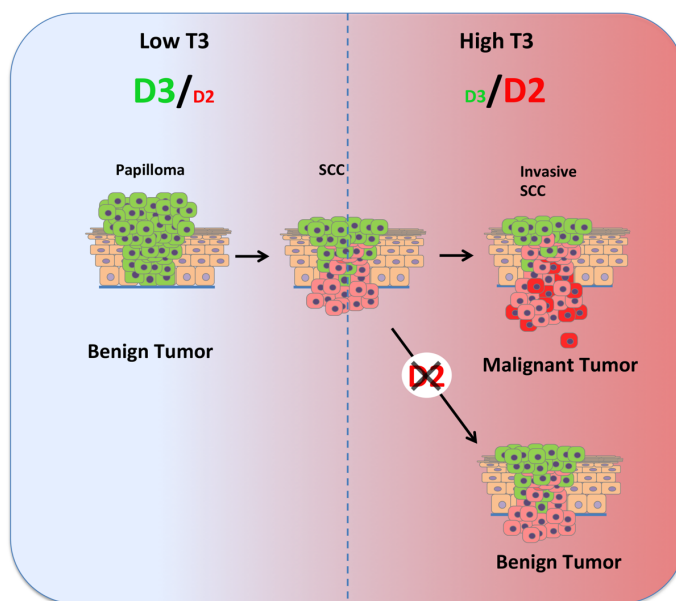


Figure 5. Graphical abstract of TH action in epithelial tumorigenesis

5. Methods

Cell Cultures and Transfections

SCC-13 cells (Cellosaurus:RRID:CVCL_4029) were derived from skin squamous cell carcinoma (NCIt: C4819), SCC 011 (Cellosaurus: RRID:CVCL_5986) were derived from laryngeal squamous cell carcinoma (NCIt: C4044) and SCC 022 (Cellosaurus: RRID:CVCL_5991) were derived from laryngeal squamous cell carcinoma (NCIt: C4044). All the cells were mycoplasma free. SCC-13 and SCC D2KO cells were cultured in keratinocyte-SFM (KSFM 1X) serum-free medium [+] L-Glu (Gibco Life Technologies) with bovine pituitary extract (30 $\mu\text{g/ml}$) and human recombinant epidermal growth factor (EGF) protein (0.24 ng/mL). SCC D3KO cells were cultured in KSFM with 4% Ca^{2+} -chelated charcoal stripped fetal bovine serum (FBS) and EGF Human Recombinant (Gibco Life Technologies). All transient transfections were performed using Lipofectamine 2000 (Life Technologies) according to the manufacturer's instructions.

Dio2 and Dio3 Targeted Mutagenesis

Targeted mutagenesis of Dio3 and Dio2 in SCC was achieved by using the CRISPR/Cas9 system from Santa Cruz Biotechnology. Control SCC cells were stably transfected with the CRISPR/Cas9 control plasmid[39]. Three days after transfection with CRISPR/Cas9 plasmids, the cells were sorted using fluorescence-activated cell sorting (FACS) for green fluorescent protein expression. Single clones were analyzed by PCR to identify alterations in coding regions, and Dio2 exon 1 was sequenced to identify the inserted mutations. All the experiments in D2- and D3KO cells were repeated in three different D3KO and three different D2KO clones to avoid off-target effects.

Real Time PCR

Cells and tissues were lysed in Trizol (Life Technologies Ltd) according to the manufacturer's protocol. 1 µg of total RNA was used to reverse transcribe cDNA using Vilo reverse transcriptase (Life Technologies Ltd), followed by Real Time qPCR using iQ5 Multicolor Real Time Detector System (BioRad) with the fluorescent double-stranded DNA-binding dye SYBR Green (Biorad).

Specific primers for each gene were designed to generate products of comparable sizes (about 200 bp for each amplification). For each reaction, standard curves for reference genes were constructed based on six four-fold serial dilutions of cDNA. All experiments were run in triplicate.

The gene expression levels were normalized to cyclophilin A and calculated as follows: $N^{*target} = 2^{(DCt\ sample - DCt\ calibrator)}$. Primer sequences are indicated in the Table 1.

Protein Extraction from Skin and Western Blot Analysis

Dorsal skin was removed from mice and immediately snap-frozen in liquid N₂. 800 µL of lysis buffer (0.125 M Tris pH 8.6; 3% SDS, protease inhibitors including PMSF 1 mM and phosphatase inhibitors) were added to all dorsal skin samples, which were then homogenized with Tissue Lyser (Qiagen). Total tissues protein or cell protein was separated by 10% SDS-PAGE followed by Western Blot. The membrane was then

blocked with 5% non-fat dry milk in PBS, probed with anti-E-cadherin, anti-N-cadherin, anti- α Flag M2, anti-vimentin, anti-D3, and anti-tubulin antibodies (loading as control) overnight at 4°C, washed, and incubated with horseradish peroxidase-conjugated anti-mouse immunoglobulin G secondary antibody (1:3000). Band detection was performed using an ECL kit (Millipore, cat. WBKLS0500). The gel images were analyzed using ImageJ software and all Western blot were run in triplicate. Antibodies are indicated in the Table 2.

Wound scratch assay

SCC CTR, D2KO and D3KO cells were seeded in p60 plates until they reached 100% confluence. Cells were then treated with mitomycin C from *Streptomyces caespitosus* (0.5 mg/ml). At time T0, a cross-shaped scratch was made on the cell monolayer with the tip of a sterile 2 μ l micropipette. The FBS-free culture medium was then replaced with fresh medium to wash out released cells. Cell migration was measured by comparing pictures taken at the beginning and the end of the experiment at the times indicated in each experiment using 10X magnification with a IX51 Olympus microscope and the Cell*F Olympus Imaging Software. ImageJ software was used to draw the cell-free region limits in each case. The initial cell-free surface was subtracted from the endpoint cell-free surface and plotted in a graph as shown in Figure 5G.

Colony Formation Assay

To evaluate colony formation, cells were seeded out in appropriate dilutions to form colonies. Five days after plating, cells were washed with PBS and stained with 1% crystal violet in 20% ethanol for 10 min at room temperature. Cells were washed twice with PBS and colonies were counted.

Invasion assay

Matrigel chambers (Corning) were used to determine the effect of D3 depletion on invasiveness as per the manufacturer's protocol. In brief, SCC CTR, D2KO and D3KO cells treated with T3 (30 nM) were harvested, re-suspended in serum-free medium, and then transferred to the hydrated Matrigel chambers (200,000 cells per well). The chambers were then incubated for 5 days in culture medium. The cells on the upper

surface were scraped off and washed away, whereas the invaded cells on the lower surface were fixed and stained with 1% crystal violet in 20% ethanol for 10 min at room temperature. Finally, invaded cells and migrated cells were counted under a microscope and the relative number was calculated.

Matrix Metalloproteinase (MMP) assays

The concentrations of MMP-2, MMP-3, MMP-7 and MMP-13 in the supernatant of SCC-CTR, SCC-CRISPD2 and SCC-CRISPD3 cells were detected via enzyme-linked assays (ELISA) according to the manufacturer's instructions (Cat No.ab100603; ab100606; ab100607; ab100608; ab100605). The absorbance at 450 nm was recorded using the VICTOR Multilabel Plate Reader. The general activity of the MMP enzyme was determined using an assay kit purchased from Abcam (Cat No. ab112146) according to the manufacturer's protocol. In brief, SCC-CTR, SCC-CRISPD2 and SCC-CRISPD3 were seeded into triplicate wells of 6-well plates and allowed to attach overnight and then starved with serum free media for another 18 h. MMP activity was assayed in the media; 25 μ l of medium was removed and added to 25 μ l of 2 mM APMA working solution and incubated for 15 min at 20°C after which 50 μ l of the green substrate solution was added. An end-point measurement was then performed for the MMP activity using a microplate reader with a filter set of Ex/Em = 490/ 525 nm.

Animals, Histology and Immunostaining

sD3KO (K14Cre^{ERT}-D3^{fl/fl}) and sD2KO (K14Cre^{ERT}-D2^{fl/fl}) mice were obtained by crossing the keratinocyte-specific conditional K14Cre^{ERT} mouse [68] with D3^{fl/fl} [59] or D2^{fl/fl} mice [69]. Depletion was induced by treatment with 10 mg of tamoxifen at different time points as indicated in each experiment. The generation of D2-3xFlag is described elsewhere [80]. Skin lesions were harvested at different time points after tamoxifen administration and DMBA-TPA treatment. For immunofluorescence and histology, dorsal skin from sD2KO, sD3KO, D2-3xFlag and control mice was embedded in paraffin, cut into 7- μ m sections, and H&E-stained. Slides were baked at 37°C, deparaffinized by xylenes, dehydrated with ethanol, rehydrated in PBS, and permeabilized by placing them

in 0.2% Triton X-100 in PBS. Antigens were retrieved by incubation in 0.1 M citrate buffer (pH 6.0) or 0.5 M Tris buffer (pH 8.0) at 95°C for 5 min. Sections were blocked in 1% BSA/0.02% Tween/PBS for 1 hour at room temperature. Primary antibodies were incubated overnight at 4°C in blocking buffer and washed in 0.2% Tween/PBS. Secondary antibodies were incubated at room temperature for 1 hour and washed in 0.2% Tween/PBS. Images were acquired with an IX51 Olympus microscope and the Cell*F Olympus Imaging Software.

Patients and Human Tissue Samples

Formalin-fixed, paraffin-embedded tissue blocks of 72 cutaneous squamous cell carcinomas (cSCCs), diagnosed and excised from May 1993 to May 2018, were retrieved from the archives of the Pathology Section of the Department of Advanced Biomedical Sciences, 'Federico II' University of Naples. Out of 72 cases, 50 males and 22 females, the age at diagnosis ranged between 36 and 95 years (mean age 76, median 77). Tumor staging (T1 to T4) according to the 8th AJCC classification was registered only for cSCCs located on head and neck skin and lip. cSCCs developing on mucosal surfaces and less than 1 cm in size were not included in this study. The clinical data and pathological features of the tumors are reported in Table 1. The study design and procedures involving tissue samples collection and handling were performed according to the Declaration of Helsinki, in agreement with the current Italian law, and to the Institutional Ethical Committee guidelines.

For immunohistochemistry of human samples, we selected a block of fixed tissue in each case, and one section of the block was stained with hematoxylin/eosin to verify the initial diagnosis; the other sections were used for immunohistochemical investigations.

Immunohistochemical analysis was performed on 4- μ m thick serial sections mounted on poly-L-lysine-coated glass slides. The sections were deparaffinized and subjected to antigen retrieval by microwave oven treatment (3 min x 4 times, in citrate buffer, pH 6); the backdrop (for blocking non-specific background staining) was removed using the universal blocking serum (Dako Diagnostics) for 15 min at room temperature. Endogenous alkaline phosphatase activity was quenched by adding levamisole to buffer AP (substrate buffer); the slides were rinsed with TRIS+Tween20 pH 7.4 buffer, and incubated in a humidified chamber with primary antibodies anti-E-cadherin (mouse

monoclonal antibody, diluted 1:300 1 h at room temperature, BD Biosciences), anti-ZEB-1 (rabbit polyclonal antibody, diluted 1:200 1 h at room temperature, NBP1-05987 Novus Biologicals, UK) and anti-D3. Then used a biotinylated secondary antibody and streptavidin conjugated with alkaline phosphatase. The reaction was visualized with chromogen fast red, which showed the presence of the antigen that we sought in red (Dako REAL Detection System, Alkaline Phosphatase/RED, Rabbit/Mouse). After weak nuclear counterstaining with hematoxylin, the sections were mounted with a synthetic medium (Entellan, Merck). Positivity for E-cadherin and ZEB-1 was visualized as red nuclear staining and red membranous staining, respectively. The level of immunostaining was scored semiquantitatively.

DMBA/TPA Carcinogenesis

The dorsal skin of 2 months old mice was treated with a single dose (100 μ L, 1 mg/ml) of the carcinogen 7,12-dimethylbenz[a]anthracene (DMBA) resuspended in propanone, followed by multiple applications of the tumor promoter 12-O-tetradecanoylphorbol-13-acetate, TPA (150 μ L, 100 μ M) in the two-stage protocol. Experiments in D3F1/F1 mice were performed using 12 CTR mice and 12 sD3KO mice. Experiments in D2F1/F1 mice were performed using a total of 30 CTR mice and 30 sD2KO mice. Experiments in D2-Flag mice were performed using 8 mice. In all the cohorts there were approximately as many female as male mice. As shown in Fig. S13, the number of metastatic organs was evaluated based on the overall expression of K8 and K14.

Isolation of TICs and Transplantation in Immunodeficient Mice

Papillomas and carcinomas arising from DMBA/TPA D2-3xFlag mice were digested in collagenase I (Sigma) for 2 h at 37°C on a rocking plate. Collagenase I activity was blocked by the addition of DMEM with 10% FBS. After tumor digestion, cells were filtered through a 70 μ m cell strainer. Immunostaining was performed using APC-anti-mouse CD34 (code 119310; Biolegend), PE-rat anti human α 6-integrin (code 555736; BD Pharmingen), FITC anti-CD3/GR-1/CD11B/CD45-B220/TER 119 (code 78022; Biolegend), vioBlu-anti mouse CD326 (code 130-102-421; Milteny Biotech) by incubation for 1 hour. Fluorescence-activated cell sorting analysis was performed using FACS Canto2 software (FACS Canto2, Becton Dickinson). Sorted cells were collected

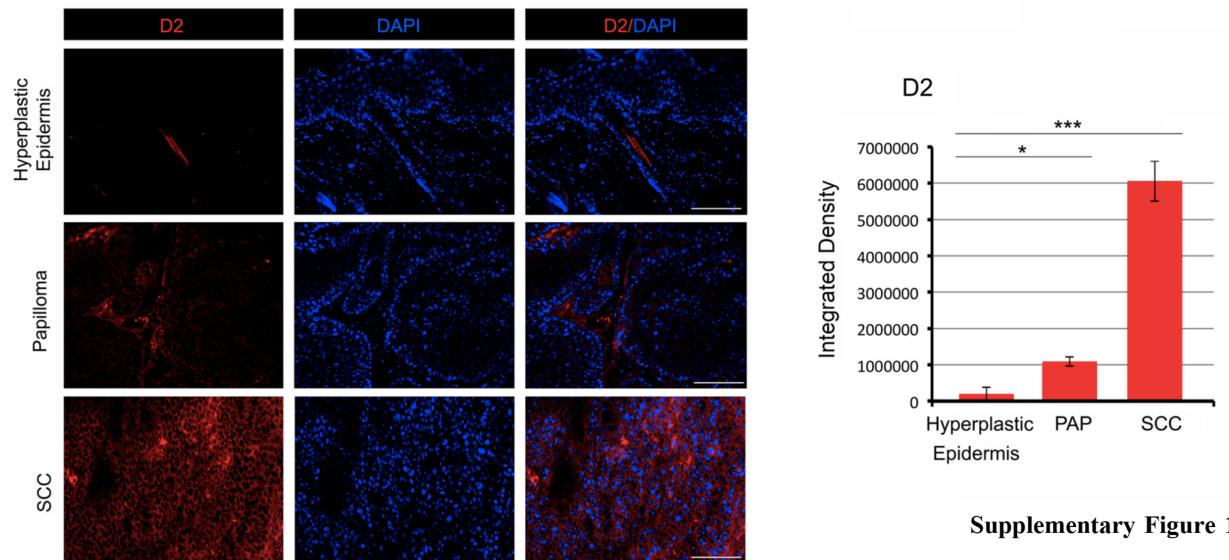
for in vivo transplantation experiments. In detail, cells were resuspended in 8% FBS with matrigel (100 μ L [8 mg/ml] Sigma) and injected subcutaneously into athymic null mice. Triplicate injections per mouse were performed. Tumor volume was calculated with the formula $V = \frac{1}{4} \pi [d^2 D]/6$, where d is the minor tumor axis and D is the major tumor axis. All animal experiments and mouse husbandry were carried out in the animal facility of CEINGE-Biotecnologie Avanzate, Naples, Italy, in accordance with institutional guidelines.

Statistics

The data are expressed as means \pm standard deviation (SD) of three independent experiments. Statistical differences and significance between samples were determined using the Student's two-tailed t test. Relative mRNA levels (in which the control sample was arbitrarily set as 1) are reported as results of real time PCR, in which the expression of cyclophilin A served as housekeeping gene. A P value < 0.05 was considered statistically significant.

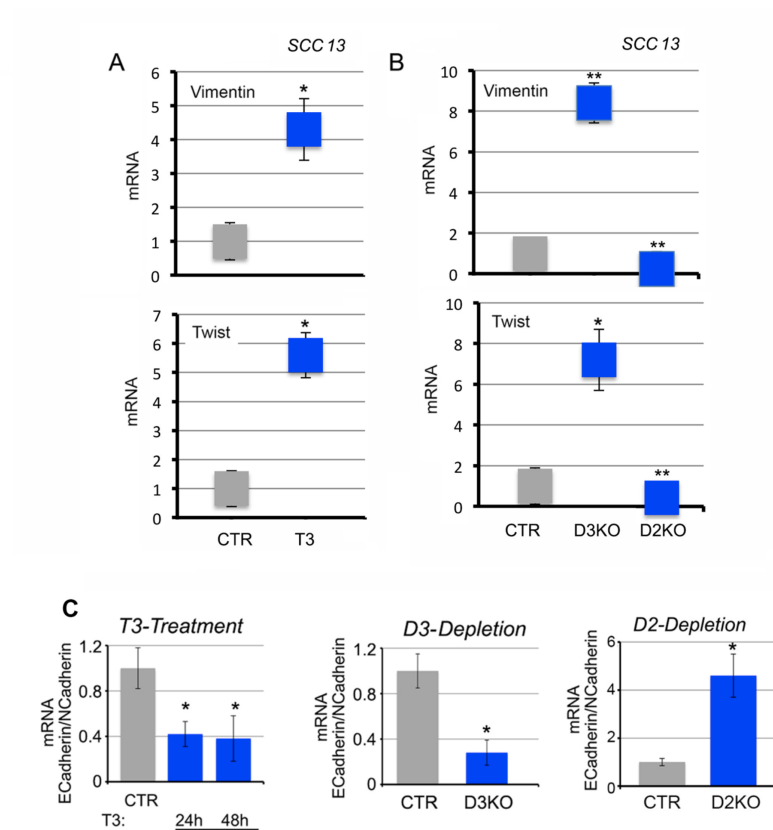
6. Supplementary informations

6.1 Supplementary Figures

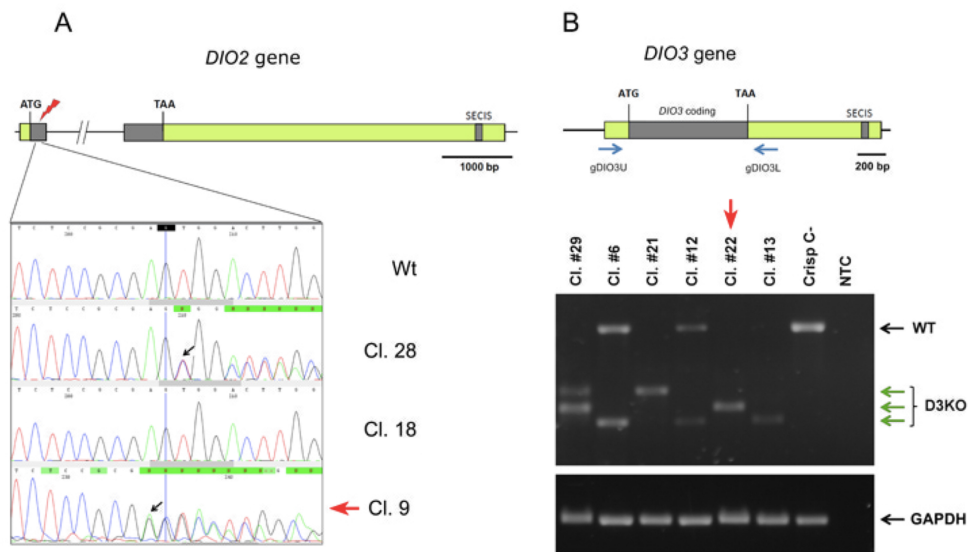


Supplementary Figure 1.

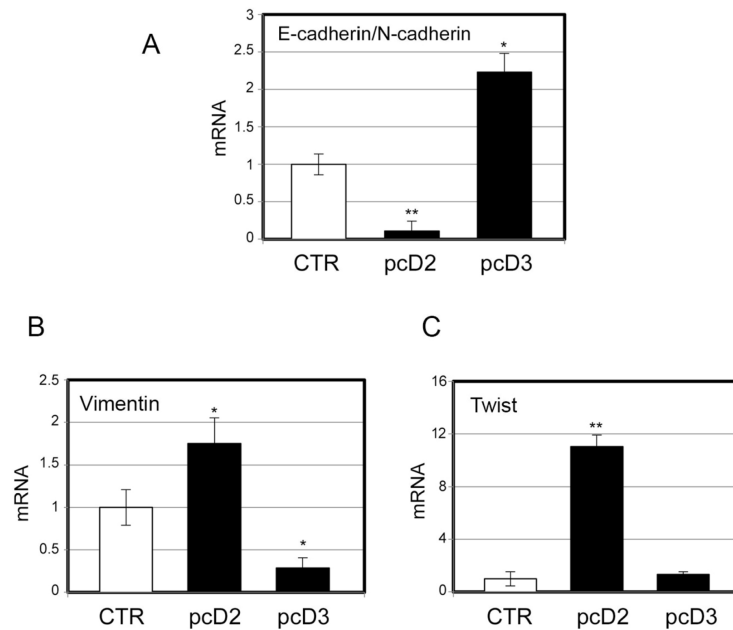
Supplementary Figure 1: *D2* expression in SCC tumorigenesis. Immunofluorescence of *D2* expression in chemically induced SCC at 12, 15 and 30 weeks after DMBA treatment. Scale bar represents 100 μ m.



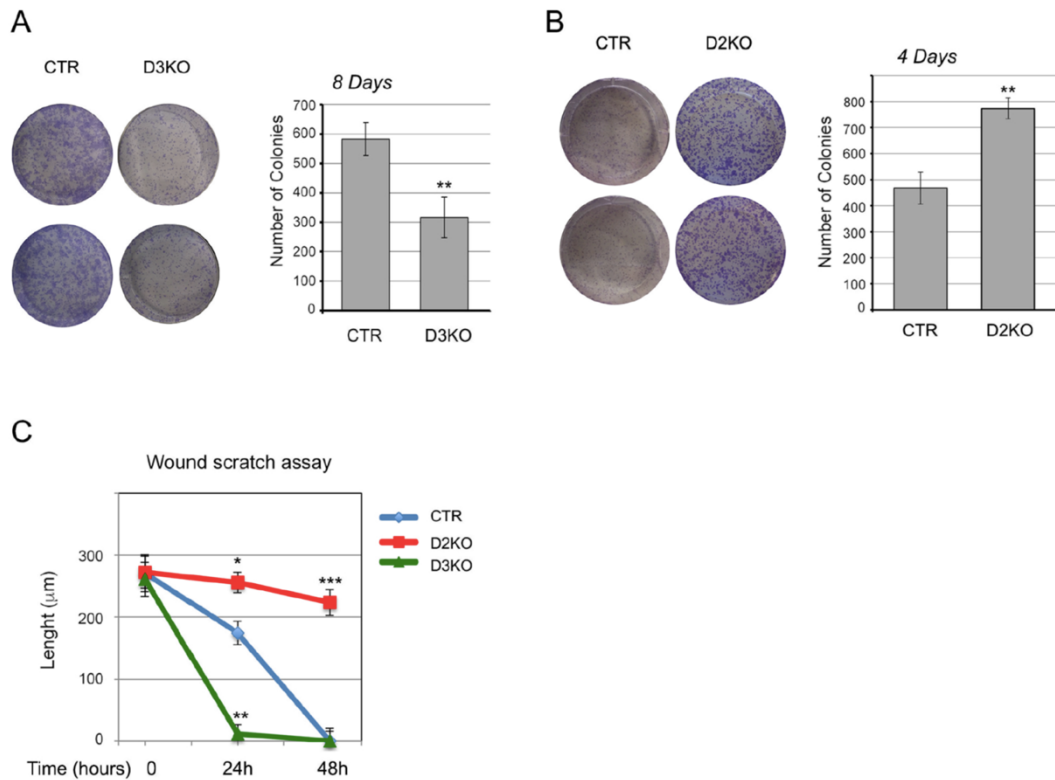
Supplementary Figure 2. *Markers of EMT are regulated by T3 and deiodinases silencing in SCC 13 cells.* (A) Vimentin and Twist mRNA expression in SCC cells treated with 30 nM T3 for 48h. (B) Vimentin and Twist mRNA in D2KO and D3KO cells compared to the control, CRISP-CTR SCC cells. (C) E-Cadherin/NCadherin ratio was evaluated by real time PCR in T3-treated and in D3KO and D2KO cells.



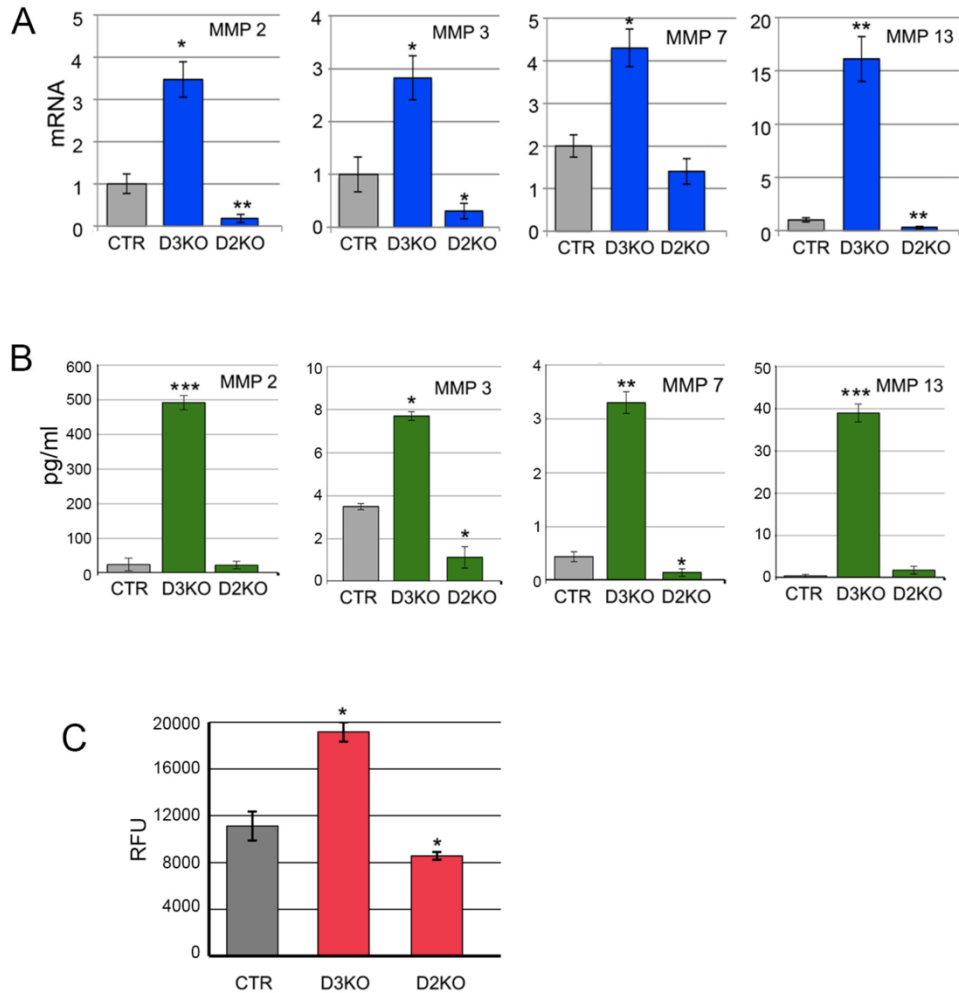
Supplementary Figure 3. *CRISPR/Cas9-mediated mutagenesis of Dio2 and Dio3 gene in SCC cells.* (A) Schematic representation of the *DIO2* locus (top). Effective mutagenesis of *DIO2* locus was assessed by genomic DNA sequencing of exon 1. Three clones are compared to WT SCC cells. The red arrow indicates the selected clone (bottom). (B) Schematic representation of the *DIO3* locus (top). Effective mutagenesis of *DIO3* locus was assessed by PCR analysis with the indicated oligonucleotides (gDIO3U and L). Six clones are compared to WT SCC cells. The green arrows indicate the mutated *DIO3* products. The red arrow indicates the selected clone (bottom).



Supplementary Figure 4. *Deiodinases overexpression regulates expression of markers of EMT.* (A) E-cadherin and Ncadherin mRNA expression and their ratio were measured by real time PCR in SCC cells transiently transfected with D2-overexpression plasmid (pcD2) and D3-overexpression plasmid (pcD3) for 48h. (BC) Vimentin and Twist mRNA levels were evaluated by real time PCR in same cells as in A.



Supplementary Figure 5. *D3* and *D2* Depletion inversely regulate proliferation and migration of SCC cells. (A, B) Clonogenic assay of CTR and D3KO (A) and CTR and D2KO (B) cells grown for 8 days (A) and 4 (B) as indicated; representative images of petri dishes are shown. Statistically significant differences were evaluated by two-way analysis of variance with the Bonferroni post-test to compare all data from D3KO clones to those from CTR. (C) Wound scratch assay was performed in CTR, D2KO and D3KO clones. Cell migration was measured as described. * $p < 0.05$, ** $p < 0.01$, and *** $p < 0.001$.



Supplementary Figure 6.D2 Depletion reduces the expression, secretion and activity of metalloproteases. (A) Metalloproteases 2, 3, 7 and 13 mRNA expression was analyzed by real time PCR in D3KO, D2KO and CTR cells. (B) Rate of secretion of Metalloproteases was measured in the culture medium of D3KO, D2KO and CTR cells. Levels of secreted Metalloproteases are expressed as pg/ml and represent an average of three different experiments performed in duplicate. (C) Enzymatic activity of Metalloproteases was measured by Elisa as indicated in Methods in D3KO, D2KO and CTR cells.

Table 1. Clinicopathological characteristics of the study population

N°	Sex	Age	Tumor site	Grading	T	N	M	Stage	Recurrence	Perineural invasion
1	M	76	scalp	G1	T1	Nx	M0	I	yes	ND
2	M	73	ear	G1	T1	Nx	M0	I	no	ND
3	F	86	cheek	ND	T2	Nx	M0	II	no	ND
4	M	68	ND	G1	T2	Nx	M0	II	no	ND
5	M	72	hand	G1	-	-	-	No staging	yes	ND
6	F	85	hand	G3	-	-	-	No staging	no	ND
7	M	67	hand	G2-G3	-	-	-	No staging	yes	ND
8	F	67	neck	G2	T3	Nx	M0	III	no	ND
9	F	71	ND	ND	T1	Nx	M0	I	no	ND
10	M	36	leg	G1	-	-	-	No staging	no	ND
11	M	49	leg	G2	-	-	-	No staging	no	ND
12	F	76	ND	G3	T2	Nx	M0	II	no	ND
13	F	76	lip	G2	T1	Nx	M0	I	no	ND
14	M	70	ear	G2	T1	Nx	M0	I	yes	ND
15	M	60	ND	G2	T2	Nx	M0	II	no	ND
16	M	67	cheek	G2-G3	T2	Nx	M0	II	no	ND
17	F	95	cheek	G2	T3	Nx	M0	III	no	ND
18	F	83	cheek	G2	T1	Nx	M0	I	no	ND
19	F	68	lip	G2	T1	Nx	M0	II	no	ND
20	M	79	scalp	G2	T3	Nx	M0	III	no	ND
21	F	51	arm	G2	-	-	-	No staging	no	ND
22	F	73	trunk	G3	-	-	-	No staging	no	yes
23	M	75	cheek	G2	T3	NX	M0	III	yes	no
24	M	77	forehead	G2-G3	T4	NX	M0	IV	no	no
25	M	77	scalp	ND	T1	NX	M0	I	yes	no

54	F	75	cheek	G1-G2	T2	NX	M0	II	no	no
55	M	75	scalp	G1-G2	T3	NX	M0	III	yes	no
56	M	85	scalp	G3	T3	NX	M0	III	yes	no
57	M	78	scalp	G3	T3	N0	M0	III	no	yes
58	M	86	cheek	G3	T3	NX	M0	III	no	yes
59	M	59	temple	G1-G2	T2	NX	M0	II	no	no
60	M	87	scalp	G1	T2	NX	M0	II	no	no
61	F	65	cheek	G3	T3	NX	M0	III	yes	yes
62	M	69	scalp	G1-G2	T1	NX	M0	I	no	no
63	M	78	ear	G1	T1	NX	M0	I	no	no
64	F	82	nose	G1	T1	NX	M0	I	no	no
65	M	86	scalp	G3	T3	NX	M0	III	no	yes
66	M	70	scalp	G1	T2	NX	M0	II	no	no
67	M	85	scalp	G3	T3	NX	M0	III	no	no
68	M	86	scalp	G3	T3	NX	M0	III	no	no
69	M	63	eyelid	G1	T1	NX	M0	I	no	no
70	F	86	nose	G1	T1	NX	M0	I	no	no
71	M	83	scalp	G2-G3	T3	NX	M0	III	no	no
72	F	87	forehead	G2	T3	N1	M1	IV	no	no

Table 2. List of oligonucleotides

Oligonucleotides used for real-time PCR		
Gene	Forward primer (5' → 3')	Reverse primer (5' → 3')
<i>Cyclophilin A (CypA)</i>	CGCCACTGTCGCTTTTCG	AACTTTGTCTGCAAACAGCTC
<i>CYCLOPHILIN A (CYP A)</i>	AGTCCATCTATGGGGAGAAAATTG	GCCTCCACAATATTCATGCCTTC
<i>Dio2</i>	CTTCCTCCTAGATGCCTACAAAC	GGCATAATTGTTACCTGATTCAGG
<i>DIO2</i>	CTCTATGACTCGGTCATTCTGC	TGTCACCTCCTTCTGTACTGG
<i>Dio3</i>	CCGCTCTCTGCTGCTTCAC	CGGATGCACAAGAAAATCTAAAAGC
<i>DIO3</i>	CCTGGGACTCTGCTTCTGTAAC	GGGGTGTAAGAAAATGCTGTAGAG
<i>E-cadherin (Cdh1)</i>	CGTCCTGCCAATCCTGATGA	ACCACTGCCCTCGTAATCGAAC
<i>E-CADHERIN (CDH1)</i>	TGTCGACCGGTGCAATCTT	GGCGCCACCTCGAGAGA
<i>Krt14</i>	GATGTGACCTCCACCAACCG	CCATCGTGCACATCCATGAC
<i>Krt6</i>	TCGTGACCCTGAAGAAGGATGTA	CCTTGGCTTGCAGTTCAACTT
<i>Krt8</i>	ACAACAAGTTTCGCCTCCTTC	TCTCCATCTCTGTACGCTTGT
<i>MMP2</i>	AAGGATGGCAAGTACGGCTT	TCATCGTAGTTGGCTGTGGT
<i>MMP3</i>	CTCCAACCGTGAGGAAAATC	CATGGAATTTCTTCTCATCAAA
<i>MMP7</i>	GGGGACTCCTACCCATTGA	TTAGGATCAGAGGAATGTCC
<i>MMP9</i>	CCTGGAGACCTGAGAACCAATC	CGGCAAGTCTTCCGAGTAGT
<i>MMP13</i>	TCTTGTTGCTGCGCATGAGT	AAGGGTCACATTTGTCTGGC
<i>N-cadherin (Cdh2)</i>	ACAGTGGAGCTCTACAAAGG	CTGAGATGGGGTTGATAATG
<i>N-CADHERIN (CDH2)</i>	ACAGTGGCCACCTACAAAGG	CCGAGATGGGGTTGATAATG
<i>TWIST</i>	CCAGCTCCAGAGTCTCTAGA	GCCAGGTACATCGACTTCT
<i>VIM</i>	GAACCTGCAGGAGGCAGAAG	CATCTTAACATTGAGCAGGTC
Oligonucleotides used for ChIP analysis		
Gene	Forward primer (5' → 3')	Reverse primer (5' → 3')
<i>VIM</i>	TGGTTCAGTCCCAGGCGGAC	CATGGTCCCCTTACTTCAGC
<i>ZEB1</i>	CGAGCATTAGACACAAGCGA	CACTCACCGTTATTGCGCC
Oligonucleotides used for genome analysis		
Gene	Forward primer (5' → 3')	Reverse primer (5' → 3')
<i>DIO3</i>	GAGTCTCCCAGCAATTGAAG	AGCCACCAAGTTCAGTCAA
<i>Dio3</i>	GTCTGGCTAACTTGAGACTCTGCT	TTGTCTTAGAACTAATCCCTTC
<i>Dio2</i>	TCAGAAGGAGACATTCTATTTC	AGGACAGAATCACTTCTTTCGAA

Table 3. List of Antibodies

ANTIBODIES	SOURCE	IDENTIFIER	DILUTION
Mouse monoclonal anti- E-cadherin	BD Biosciences	610181	1:500 IF 1:1000 WB
Rabbit polyclonal anti- N-cadherin	Elabscience	E-AB-32170	1:500 WB
Rabbit monoclonal anti-Vimentin	ABCAM	ab-92547	1:2000 WB 1:1000 IF
Rabbit polyclonal anti- α Tubulin	Santa Cruz Biotechnology	SC-5546	1:10000 WB
Mouse monoclonal anti- α Tubulin	Santa Cruz Biotechnology	SC-8035	1:10000 WB
Mouse monoclonal anti-FlagM2	SIGMA	Cat#F3165	1:1000 IF 1:1000 WB
Rabbit polyclonal anti-cytokeratin 14	COVANCE	D14IF01918	1:2000 IF
Rabbit polyclonal anti-CXCR4	ABCAM	ab-2074	1:300 IF
Rabbit polyclonal anti-cytokeratin 6	COVANCE	PRB-169P	1:1000 IF
Rat anti-cytokeratin 8 (TROMA 1)	Hybridoma bank	AB_531826	1:300 IF
Anti-D3 718	Homemade	Homemade	1:500 IF 1:500 IHC
Anti-D3 717	Homemade	Homemade	1:500 WB
Anti-Phalloidin-TRITC labeled	SIGMA	77418-1EA	1:2000 IF
Rabbit polyclonal Anti-ZEB1	ABCAM	ab-155249	1:500 WB
Rabbit polyclonal Anti-ZEB1	Novus Bio	NBP1-05987	1:250 IF 1:250 IHC
Anti-Thyroid hormone receptor antibody (C3)-Chip Grade	ABCAM	ab-2743	2,5 μ g
Anti-Thyroid hormone receptor beta antibody Chip Grade	ABCAM	ab-5622	2,5 μ g
Rabbit polyclonal anti-GAPDH	Elabscience	E-AB-20059	1:5000 WB

7. References

1. Dotto, G.P. and A.K. Rustgi, *Squamous Cell Cancers: A Unified Perspective on Biology and Genetics*. Cancer Cell, 2016. **29**(5): p. 622-637.
2. Alam, M. and D. Ratner, *Cutaneous squamous-cell carcinoma*. N Engl J Med, 2001. **344**(13): p. 975-83.
3. Herbst, R.S., J.V. Heymach, and S.M. Lippman, *Lung cancer*. N Engl J Med, 2008. **359**(13): p. 1367-80.
4. Leemans, C.R., B.J. Braakhuis, and R.H. Brakenhoff, *The molecular biology of head and neck cancer*. Nat Rev Cancer, 2011. **11**(1): p. 9-22.
5. Bray, F., et al., *Incidence trends of adenocarcinoma of the cervix in 13 European countries*. Cancer Epidemiol Biomarkers Prev, 2005. **14**(9): p. 2191-9.
6. Malik, R.D., et al., *Squamous cell carcinoma of the prostate*. Rev Urol, 2011. **13**(1): p. 56-60.
7. Tunio, M.A., et al., *Primary squamous cell carcinoma of thyroid: a case report and review of literature*. Head Neck Oncol, 2012. **4**: p. 8.
8. Dotto, G.P., *Multifocal epithelial tumors and field cancerization: stroma as a primary determinant*. J Clin Invest, 2014. **124**(4): p. 1446-53.
9. Junttila, M.R. and F.J. de Sauvage, *Influence of tumour micro-environment heterogeneity on therapeutic response*. Nature, 2013. **501**(7467): p. 346-54.
10. Elkabets, M., et al., *AXL mediates resistance to PI3Kalpha inhibition by activating the EGFR/PKC/mTOR axis in head and neck and esophageal squamous cell carcinomas*. Cancer Cell, 2015. **27**(4): p. 533-46.
11. Karia, P.S., J. Han, and C.D. Schmults, *Cutaneous squamous cell carcinoma: estimated incidence of disease, nodal metastasis, and deaths from disease in the United States, 2012*. J Am Acad Dermatol, 2013. **68**(6): p. 957-66.
12. Owens, D.M. and F.M. Watt, *Contribution of stem cells and differentiated cells to epidermal tumours*. Nat Rev Cancer, 2003. **3**(6): p. 444-51.
13. Perez-Losada, J. and A. Balmain, *Stem-cell hierarchy in skin cancer*. Nat Rev Cancer, 2003. **3**(6): p. 434-43.
14. Abel, E.L., et al., *Multi-stage chemical carcinogenesis in mouse skin: fundamentals and applications*. Nat Protoc, 2009. **4**(9): p. 1350-62.
15. Quintanilla, M., et al., *Carcinogen-specific mutation and amplification of Ha-ras during mouse skin carcinogenesis*. Nature, 1986. **322**(6074): p. 78-80.
16. Balmain, A., et al., *Activation of the mouse cellular Harvey-ras gene in chemically induced benign skin papillomas*. Nature, 1984. **307**(5952): p. 658-60.
17. Bizub, D., A.W. Wood, and A.M. Skalka, *Mutagenesis of the Ha-ras oncogene in mouse skin tumors induced by polycyclic aromatic hydrocarbons*. Proc Natl Acad Sci U S A, 1986. **83**(16): p. 6048-52.
18. Shackleton, M., et al., *Heterogeneity in cancer: cancer stem cells versus clonal evolution*. Cell, 2009. **138**(5): p. 822-9.
19. Nguyen, L.V., et al., *Cancer stem cells: an evolving concept*. Nat Rev Cancer, 2012. **12**(2): p. 133-43.
20. Reya, T., et al., *Stem cells, cancer, and cancer stem cells*. Nature, 2001. **414**(6859): p. 105-11.

21. Pardal, R., M.F. Clarke, and S.J. Morrison, *Applying the principles of stem-cell biology to cancer*. Nat Rev Cancer, 2003. **3**(12): p. 895-902.
22. Lobo, N.A., et al., *The biology of cancer stem cells*. Annu Rev Cell Dev Biol, 2007. **23**: p. 675-99.
23. Driessens, G., et al., *Defining the mode of tumour growth by clonal analysis*. Nature, 2012. **488**(7412): p. 527-30.
24. Schepers, A.G., et al., *Lineage tracing reveals Lgr5+ stem cell activity in mouse intestinal adenomas*. Science, 2012. **337**(6095): p. 730-5.
25. Malanchi, I., et al., *Cutaneous cancer stem cell maintenance is dependent on beta-catenin signalling*. Nature, 2008. **452**(7187): p. 650-3.
26. Nieto, M.A., et al., *Emt: 2016*. Cell, 2016. **166**(1): p. 21-45.
27. Brabletz, T., *To differentiate or not--routes towards metastasis*. Nat Rev Cancer, 2012. **12**(6): p. 425-36.
28. Puisieux, A., T. Brabletz, and J. Caramel, *Oncogenic roles of EMT-inducing transcription factors*. Nat Cell Biol, 2014. **16**(6): p. 488-94.
29. Huang, R.Y., et al., *An EMT spectrum defines an anoikis-resistant and spheroidogenic intermediate mesenchymal state that is sensitive to e-cadherin restoration by a src-kinase inhibitor, saracatinib (AZD0530)*. Cell Death Dis, 2013. **4**: p. e915.
30. Jordan, N.V., G.L. Johnson, and A.N. Abell, *Tracking the intermediate stages of epithelial-mesenchymal transition in epithelial stem cells and cancer*. Cell Cycle, 2011. **10**(17): p. 2865-73.
31. Pastushenko, I., et al., *Identification of the tumour transition states occurring during EMT*. Nature, 2018. **556**(7702): p. 463-468.
32. Mani, S.A., et al., *The epithelial-mesenchymal transition generates cells with properties of stem cells*. Cell, 2008. **133**(4): p. 704-15.
33. Morel, A.P., et al., *Generation of breast cancer stem cells through epithelial-mesenchymal transition*. PLoS One, 2008. **3**(8): p. e2888.
34. Fidler, I.J., *The pathogenesis of cancer metastasis: the 'seed and soil' hypothesis revisited*. Nat Rev Cancer, 2003. **3**(6): p. 453-8.
35. Friesema, E.C., et al., *Thyroid hormone transporters*. Vitam Horm, 2005. **70**: p. 137-67.
36. Gereben, B., et al., *Cellular and molecular basis of deiodinase-regulated thyroid hormone signaling*. Endocr Rev, 2008. **29**(7): p. 898-938.
37. Arrojo, E.D.R. and A.C. Bianco, *Type 2 deiodinase at the crossroads of thyroid hormone action*. Int J Biochem Cell Biol, 2011. **43**(10): p. 1432-41.
38. Gereben, B., et al., *Selective proteolysis of human type 2 deiodinase: a novel ubiquitin-proteasomal mediated mechanism for regulation of hormone activation*. Mol Endocrinol, 2000. **14**(11): p. 1697-708.
39. Miro, C., et al., *The Concerted Action of Type 2 and Type 3 Deiodinases Regulates the Cell Cycle and Survival of Basal Cell Carcinoma Cells*. Thyroid, 2017. **27**(4): p. 567-576.
40. Burmeister, L.A., J. Pachucki, and D.L. St Germain, *Thyroid hormones inhibit type 2 iodothyronine deiodinase in the rat cerebral cortex by both pre- and posttranslational mechanisms*. Endocrinology, 1997. **138**(12): p. 5231-7.

41. Salvatore, D., et al., *Type 3 Iodothyronine deiodinase: cloning, in vitro expression, and functional analysis of the placental selenoenzyme*. J Clin Invest, 1995. **96**(5): p. 2421-30.
42. Kaplan, M.M. and K.A. Yaskoski, *Phenolic and tyrosyl ring deiodination of iodothyronines in rat brain homogenates*. J Clin Invest, 1980. **66**(3): p. 551-62.
43. Bates, J.M., D.L. St Germain, and V.A. Galton, *Expression profiles of the three iodothyronine deiodinases, D1, D2, and D3, in the developing rat*. Endocrinology, 1999. **140**(2): p. 844-51.
44. Huang, S.A., et al., *Type 3 iodothyronine deiodinase is highly expressed in the human uteroplacental unit and in fetal epithelium*. J Clin Endocrinol Metab, 2003. **88**(3): p. 1384-8.
45. Beatson, G.T., *On the Treatment of Inoperable Cases of Carcinoma of the Mamma: Suggestions for a New Method of Treatment, with Illustrative Cases*. Trans Med Chir Soc Edinb, 1896. **15**: p. 153-179.
46. Meyer, E.L., M.S. Wagner, and A.L. Maia, *[Iodothyronine deiodinases expression in thyroid neoplasias]*. Arq Bras Endocrinol Metabol, 2007. **51**(5): p. 690-700.
47. Piekielko-Witkowska, A. and A. Nauman, *Iodothyronine deiodinases and cancer*. J Endocrinol Invest, 2011. **34**(9): p. 716-28.
48. Casula, S. and A.C. Bianco, *Thyroid hormone deiodinases and cancer*. Front Endocrinol (Lausanne), 2012. **3**: p. 74.
49. Dentice, M., D. Antonini, and D. Salvatore, *Type 3 deiodinase and solid tumors: an intriguing pair*. Expert Opin Ther Targets, 2013. **17**(11): p. 1369-79.
50. Huang, S.A., et al., *Severe hypothyroidism caused by type 3 iodothyronine deiodinase in infantile hemangiomas*. N Engl J Med, 2000. **343**(3): p. 185-9.
51. Huang, S.A., et al., *A 21-year-old woman with consumptive hypothyroidism due to a vascular tumor expressing type 3 iodothyronine deiodinase*. J Clin Endocrinol Metab, 2002. **87**(10): p. 4457-61.
52. Weber Pasa, M., et al., *Consumptive Hypothyroidism: Case Report of Hepatic Hemangioendotheliomas Successfully Treated with Vincristine and Systematic Review of the Syndrome*. Eur Thyroid J, 2017. **6**(6): p. 321-327.
53. Aw, D.K., et al., *Studies of molecular mechanisms associated with increased deiodinase 3 expression in a case of consumptive hypothyroidism*. J Clin Endocrinol Metab, 2014. **99**(11): p. 3965-71.
54. Kaplan, M.M., et al., *Human epidermal keratinocytes in culture convert thyroxine to 3,5,3'-triiodothyronine by type II iodothyronine deiodination: a novel endocrine function of the skin*. J Clin Endocrinol Metab, 1988. **66**(4): p. 815-22.
55. Santini, F., et al., *Role for inner ring deiodination preventing transcutaneous passage of thyroxine*. J Clin Endocrinol Metab, 2003. **88**(6): p. 2825-30.
56. Sellheyer, K., *Basal cell carcinoma: cell of origin, cancer stem cell hypothesis and stem cell markers*. Br J Dermatol, 2011. **164**(4): p. 696-711.
57. Dentice, M., et al., *Sonic hedgehog-induced type 3 deiodinase blocks thyroid hormone action enhancing proliferation of normal and malignant keratinocytes*. Proc Natl Acad Sci U S A, 2007. **104**(36): p. 14466-71.

58. Luongo, C., et al., *The sonic hedgehog-induced type 3 deiodinase facilitates tumorigenesis of basal cell carcinoma by reducing Gli2 inactivation*. *Endocrinology*, 2014. **155**(6): p. 2077-88.
59. Di Girolamo, D., et al., *Reciprocal interplay between thyroid hormone and microRNA-21 regulates hedgehog pathway-driven skin tumorigenesis*. *J Clin Invest*, 2016. **126**(6): p. 2308-20.
60. Mori, K., et al., *Thyroxine 5-deiodinase in human brain tumors*. *J Clin Endocrinol Metab*, 1993. **77**(5): p. 1198-202.
61. Murakami, M., et al., *Expression of type II iodothyronine deiodinase in brain tumors*. *J Clin Endocrinol Metab*, 2000. **85**(11): p. 4403-6.
62. Nauman, P., et al., *The concentration of thyroid hormones and activities of iodothyronine deiodinases are altered in human brain gliomas*. *Folia Neuropathol*, 2004. **42**(2): p. 67-73.
63. Canettieri, G., et al., *Isolation of human type 2 deiodinase gene promoter and characterization of a functional cyclic adenosine monophosphate response element*. *Endocrinology*, 2000. **141**(5): p. 1804-13.
64. Curcio, C., et al., *The human type 2 iodothyronine deiodinase is a selenoprotein highly expressed in a mesothelioma cell line*. *J Biol Chem*, 2001. **276**(32): p. 30183-7.
65. Gouveia, C.H., et al., *Type 2 iodothyronine selenodeiodinase is expressed throughout the mouse skeleton and in the MC3T3-E1 mouse osteoblastic cell line during differentiation*. *Endocrinology*, 2005. **146**(1): p. 195-200.
66. Lehrbach, D.M., M.E. Nita, and I. Cecconello, *Molecular aspects of esophageal squamous cell carcinoma carcinogenesis*. *Arq Gastroenterol*, 2003. **40**(4): p. 256-61.
67. Dentice, M., et al., *beta-Catenin regulates deiodinase levels and thyroid hormone signaling in colon cancer cells*. *Gastroenterology*, 2012. **143**(4): p. 1037-47.
68. Lapouge, G., et al., *Skin squamous cell carcinoma propagating cells increase with tumour progression and invasiveness*. *EMBO J*, 2012. **31**(24): p. 4563-75.
69. Luongo, C., et al., *The selective loss of the type 2 iodothyronine deiodinase in mouse thyrotrophs increases basal TSH but blunts the thyrotropin response to hypothyroidism*. *Endocrinology*, 2015. **156**(2): p. 745-54.
70. Brabletz, S. and T. Brabletz, *The ZEB/miR-200 feedback loop--a motor of cellular plasticity in development and cancer?* *EMBO Rep*, 2010. **11**(9): p. 670-7.
71. Caramel, J., M. Ligier, and A. Puisieux, *Pleiotropic Roles for ZEB1 in Cancer*. *Cancer Res*, 2018. **78**(1): p. 30-35.
72. Dentice, R.L., M.R. Elkins, and P.T. Bye, *Adults with cystic fibrosis prefer hypertonic saline before or during airway clearance techniques: a randomised crossover trial*. *J Physiother*, 2012. **58**(1): p. 33-40.
73. Camp, R.L., M. Dolled-Filhart, and D.L. Rimm, *X-tile: a new bio-informatics tool for biomarker assessment and outcome-based cut-point optimization*. *Clin Cancer Res*, 2004. **10**(21): p. 7252-9.

74. Cohen, J., et al., *Attenuated transforming growth factor beta signaling promotes nuclear factor-kappaB activation in head and neck cancer*. *Cancer Res*, 2009. **69**(8): p. 3415-24.
75. Chung, C.H., et al., *Molecular classification of head and neck squamous cell carcinomas using patterns of gene expression*. *Cancer Cell*, 2004. **5**(5): p. 489-500.
76. Li, X., et al., *Intrinsic resistance of tumorigenic breast cancer cells to chemotherapy*. *J Natl Cancer Inst*, 2008. **100**(9): p. 672-9.
77. Krashin, E., et al., *Thyroid Hormones and Cancer: A Comprehensive Review of Preclinical and Clinical Studies*. *Front Endocrinol (Lausanne)*, 2019. **10**: p. 59.
78. Dentice, M., et al., *The deiodinases and the control of intracellular thyroid hormone signaling during cellular differentiation*. *Biochim Biophys Acta*, 2013. **1830**(7): p. 3937-45.
79. Sagliocchi, S., et al., *The thyroid hormone activating enzyme, type 2 deiodinase, induces myogenic differentiation by regulating mitochondrial metabolism and reducing oxidative stress*. *Redox Biol*, 2019. **24**: p. 101228.
80. Castagna, M.G., et al., *DIO2 Thr92Ala Reduces Deiodinase-2 Activity and Serum-T3 Levels in Thyroid-Deficient Patients*. *J Clin Endocrinol Metab*, 2017. **102**(5): p. 1623-1630.